CALIPSO Level 3 Stratospheric Aerosol Product: Version 1.00 Algorithm Description and Initial Assessment

Jayanta Kar[1,2], Kam-Pui Lee[1,2], Mark A. Vaughan[2], Jason L. Tackett[1,2], Charles R. Trepte[2], David M. Winker[2], Patricia L. Lucker[1,2], Brian J. Getzewich[1,2]

[1]Science Systems and Applications Inc., Hampton, VA, USA
[2]NASA Langley Research Center, Hampton, VA, USA

Correspondence to: J. Kar (jayanta.kar@nasa.gov)

Abstract. In August 2018, the Cloud-Aerosol Lidar and Infrared Pathfinder Satellite Observation (CALIPSO) project released a new level 3 stratospheric aerosol profile data product derived from nearly 12 years of measurements acquired by the space-borne Cloud-Aerosol Lidar with Orthogonal Polarization (CALIOP). This monthly averaged, gridded level 3 product is based on version 4.2 of the CALIOP level 1 and level 2 data products, which feature significantly improved calibration that now makes it possible to reliably retrieve profiles of stratospheric aerosol extinction and backscatter coefficients. This paper describes the science algorithm and data handling techniques that were developed to generate the CALIPSO version 1.00 level 3 stratospheric aerosol profile product. Further, we show that the retrieved extinction profiles capture the major stratospheric perturbations over the last decade resulting from volcanic eruptions, extreme smoke events, and signatures of stratospheric dynamics. Initial assessment of the product by inter-comparison with the stratospheric aerosol retrievals from the Stratospheric Aerosol and Gas Experiment III (SAGE III) on the International Space Station (ISS) indicates good agreement in the tropical stratospheric aerosol layer (30^{o}N-30^{o}S), where the average difference between zonal mean extinction profiles is typically less than 25% between 20 km and 30 km. However, differences can exceed 100% in the very low aerosol loading regimes found above 25 km at higher latitudes.

1. Introduction.

While the bulk of the global distribution of atmospheric aerosols is concentrated within the planetary boundary layer and free troposphere, the persistent aerosol burden in the stratosphere has long been known to have important implications for Earth's climate (Turco et al., 1980). Techniques for reliable detection of a background aerosol layer in the stratosphere date back to the early sixties (Junge and Manson, 1961). These aerosols are mostly liquid sulfate particles which are derived from precursor gases like SO_2 and carbonyl sulfide (OCS) transported from the troposphere (Thomason and Peter, 2006, Kremser et al., 2016, Thomason et al., 2018). In addition, intermittent volcanic eruptions and strong biomass burning events can inject sulfates, ash, and smoke into the stratosphere, which can last for long periods of time and exert significant climatic influences. For example, stratospheric perturbations from the Pinatubo volcano in 1991 lasted for several years (Chazette et al., 1995, Robock, 2000, Deshler, 2008). While eruptions of the same scale as Pinatubo have not taken place in the last 25 years or so, there is evidence that a large number of smaller eruptions have been significantly affecting the stratosphere with implications for the climate system (Vernier et al., 2011, Solomon et al., 2011). Thus it is very important to monitor the stratospheric aerosol loading over the long term. As such, stratospheric aerosol measurements have been made from ground based lidar, balloon borne as well as aircraft measurements for a long time (Northam et al., 1974, Hoffman et al., 1975, McCormick et al., 1984, Brock et al., 1993, Beyerle et al., 1994, Jaeger and Deshler 2002).

Most of our current knowledge of the global distribution of stratospheric aerosols comes from satellite measurements and in particular from the Stratospheric Aerosol and Gas Experiment (SAGE) series of instruments (Mauldin et al., 1985; Chu et al., 1993; Damadeo et al., 2013). The basic principle employed in these instruments is solar occultation, wherein the vertical profile of stratospheric aerosols is retrieved from measurement of sunlight as the rays pass through the atmosphere during sunrise and sunset events as observed from the orbiting spacecraft. Stratospheric aerosols have been characterized using this technique from SAGE instruments on Earth Radiation Budget Satellite (ERBS) and Meteor-3M as well as from the International Space Station (ISS). Another space-borne instrument that uses this technique is Measurement of Aerosol Extinction in the Stratosphere and Troposphere Retrieved by Occultation (MAESTRO, McElroy et al., 2009). In addition, the Optical Spectrograph and InfraRed Imager System (OSIRIS) and the

Ozone Mapping and Profiler Suite (OMPS) have used a limb scatter technique to obtain the aerosol extinction profiles (Bourassa et al., 2012, Chen et al., 2018).

A novel and pioneering technique to retrieve aerosol profiles from space came about with the launch of the Cloud-Aerosol Lidar and Infrared Pathfinder Satellite Observation (CALIPSO) mission in April 2006, with a two-wavelength, polarization-sensitive elastic backscatter lidar as the primary payload (Winker et al., 2010). For over 12 years the Cloud-Aerosol Lidar with Orthogonal Polarization (CALIOP) has been providing profiles of aerosol and cloud extinction globally. The primary measurement from a space-borne elastic backscatter lidar consists of attenuated backscatter measurements from the aerosols and clouds in the atmosphere. The strong backscatter from the tropospheric aerosols, combined with CALIOP's relatively strong signal-to-noise ratio (SNR), has been exploited to provide accurate extinction profiles in the troposphere (Young and Vaughan, 2009, Winker et al., 2013, Young et al., 2013, 2016, 2018). In comparison, the aerosol loading in the stratosphere is much lower with correspondingly smaller SNR. As such, retrieving stratospheric aerosol information was not originally a principal target of the CALIPSO mission. However, early results indicated that it might be possible to obtain such information with adequate averaging of the data (Thomason and Pitts, 2007, Vernier et al., 2009).

One of the issues impacting the retrieval of stratospheric aerosol extinction was the realization that the standard calibration altitude of CALIOP, which was originally fixed at 30-34 km (Powell et al., 2009), was not completely free of aerosols and thus applying the molecular normalization technique at these altitudes would bias the aerosol extinction profiles (Vernier et al., 2009). This issue has since been addressed with the release of the version 4 (V4) family of CALIPSO data products in November 2016. In this version, the calibration altitude for the nighttime 532 nm data which is the primary calibration for all of CALIOP measurements (all the other measurements like the daytime data as well as the 1064 nm data are calibrated relative to the 532 nm nighttime calibration) was raised to 36-39 km, where the aerosol loading is expected to be negligible (Kar et al., 2018). This largely removed the aerosol contamination issue making reliable retrievals of stratospheric aerosols possible. Accordingly, a stand-alone CALIPSO stratospheric aerosol product was developed which uses the V4 level 1 and level 2 data from the CALIOP measurements. This is a level 3 monthly averaged product gridded in latitude (5^o), longitude (20^o) and altitude (900 m). In what follows, we describe the overall algorithm and its implementation in detail in section 2. Section 3 then presents a comprehensive assessment of the quality and capabilities of this new data product, including analyses of the temporal and spatial evolution of specific stratospheric features captured by the product and inter-comparisons with extinction retrievals from SAGE III on ISS. Discussion and concluding remarks are given in section 4 and section 5 respectively.

2. Overall design of the stratospheric aerosol profile product

2.1 Motivation for a CALIPSO stratospheric product

The CALIPSO stratospheric aerosol product is built primarily from the V4 level 1 532 nm attenuated backscatter profiles. As mentioned above, the most fundamental change in V4 level 1 data was the new calibration of the 532 nm nighttime data (Kar et al., 2018). The consequences of this change are illustrated in Figure 1, which shows the zonally averaged attenuated scattering ratios at 30-34 km from V4 for the month of May 2009.

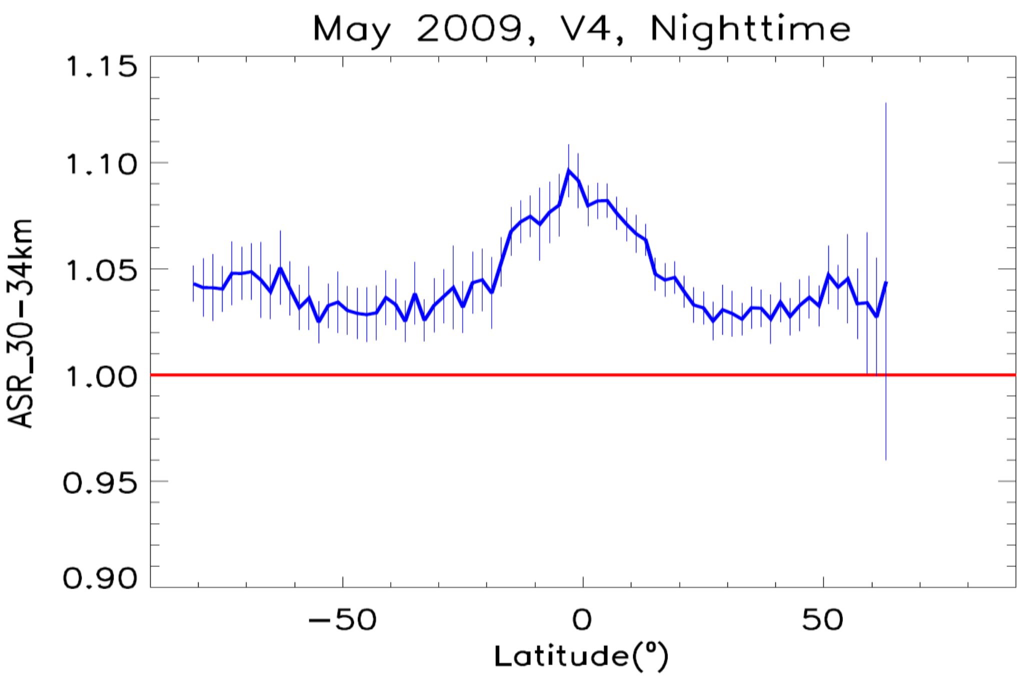

Figure 1. Zonally and vertically (over 30-34 km) averaged 532 nm attenuated scattering ratios for May 2009 nighttime data from V4 (blue). Data over the South Atlantic Anomaly were excluded. The data are binned over 2° in latitude and the error bars represent the standard error of the mean scattering ratios over this latitude interval.

As shown in Eq. (1), the attenuated scattering ratios, $R'(z)$, are computed as the ratio of the measured attenuated backscatter coefficients, $\beta'_{measured}(z)$ which contain contributions from both molecular and particulate backscatter ($\beta_m(z)$ and $\beta_p(z)$, respectively), and the attenuated backscatter coefficients calculated from modeled profiles of molecular number densities, $\beta'_{modeled}(z)$ (Vaughan et al., 2009).

$$R'(z) = \frac{\beta'_{measured}(z)}{\beta'_{modeled}(z)} = \frac{\left(\beta_m(z) + \beta_p(z)\right) T_m^2(z)\ T_{O_3}^2(z)\ T_p^2(z)}{\beta_{m,modeled}(z)\ T_{m,modeled}^2(z)\ T_{O_3,modeled}^2(z)} = \left(1 + \frac{\beta_p(z)}{\beta_{m,modeled}(z)}\right) T_p^2(z) \qquad (1)$$

In this expression, $T_X^2(z)$ represents the two-way transmittance (i.e., signal attenuation) between the lidar and altitude z for air molecules (X = m), ozone (X = O_3), and particulates (X = p). In version 3 (V3), the calibration region was fixed at 30-34 km, with the assumption that the aerosol loading in this region was negligible (Powell et al., 2009); i.e., $\beta_p(z) \approx 0$ and $T_p^2(z) = 1$. This assumption essentially forces the V3 attenuated scattering ratios in the region to one. For the V4 data release, the calibration region was raised to 36-39 km, with the concomitant assumption that the mean scattering ratio at these higher altitudes is 1.01 ± 0.01. The V4 data attenuated scattering ratios now (correctly) show significant aerosol in the altitude region used for the V3 calibration, with a maximum appearing over the tropics (Figure 1). The V4 data also capture the seasonal variation of these scattering ratios (Kar et al., 2018, see their Figure 12). This improved calibration in V4, now accurate to about 1%, provides the motivation for the development of the CALIPSO stratospheric product, as it enables the retrieval of aerosol extinction coefficients in regions previously (but incorrectly) assumed to be aerosol-free.

2.2 Design and algorithm description

The level 3 stratospheric aerosol profile product reports height-resolved monthly mean profiles of aerosol backscatter and extinction coefficients on a uniform spatial grid that extends 5° in latitude (from 85°N to 85°S), 20° in longitude (from 180°W to 180°E), and 900 m in altitude. This grid was chosen to allow for adequate averaging of the data to compensate for the lower SNR in the stratosphere while retaining some level of zonal information. Note that the range of altitudes to be covered in the stratosphere at various latitudes is from 8.2 km to 36 km, the latter being the lower limit of the calibration region. The altitude resolution of the CALIOP level 1 profiles varies over this altitude range, going from 60 m between 8.2 km and 20.2 km to 180 m between 20.2 km and 30.1 km and finally to 300 m between 30.1 km and 40 km. In order to achieve a uniform altitude resolution, the vertical grid resolution was set to 900 m. In the current version of the stratospheric aerosol product we use only nighttime data as they have significantly better SNR as compared to the daytime data (Hunt et al., 2009).

Each level 3 stratospheric aerosol file reports two distinct realizations of the monthly averaged data products. The first of these is the “background” mode, which is designed to represent the long-term background stratospheric aerosol loading. In order to achieve this, we need to remove all readily detectable perturbations within the stratosphere; i.e., overshooting cirrus clouds, polar stratospheric clouds (PSCs), and strongly scattering injections of smoke, volcanic ash, and other aerosol species which are detected using the layer detection algorithm implemented in the CALIOP level 2 data processing (Vaughan et al., 2009). The second realization is the “all aerosols” mode which is designed to represent the time history of aerosol loading in the stratosphere resulting from all possible sources. In this case, the cirrus clouds and PSCs are still removed, exactly as is done for the background mode, but, subject to various quality assurance tests, the aerosol layers detected in the level 2 analyses are retained. Details of the averaging algorithms and the various data filtering schemes are provided in the following sections.

2.2.1 Gridding and filtering

The overall design of the product is shown in Figure 2. To begin with, three input files are required for each granule under consideration. A CALIOP granule comprises half an orbit of data either from the daytime or the nighttime part of the orbit and divided by the day-night terminator. As noted in section 1, the primary input files used for this product is the lidar level 1B file, with the corresponding level 2 5 km merged layer and PSC mask files (Pitts et al., 2009) used for filtering. While the level 1B and level 2 merged layer files are based on V4, the currently available level 2 PSC files are based on V3. The latter is only available as a daily file and not for each granule separately. The 5 km merged layer file is a new product in V4 that reports the locations of all aerosol and cloud layers detected at both 5 km (also 20 km and 80 km) and single shot (333m) resolution (Vaughan et al., 2016).

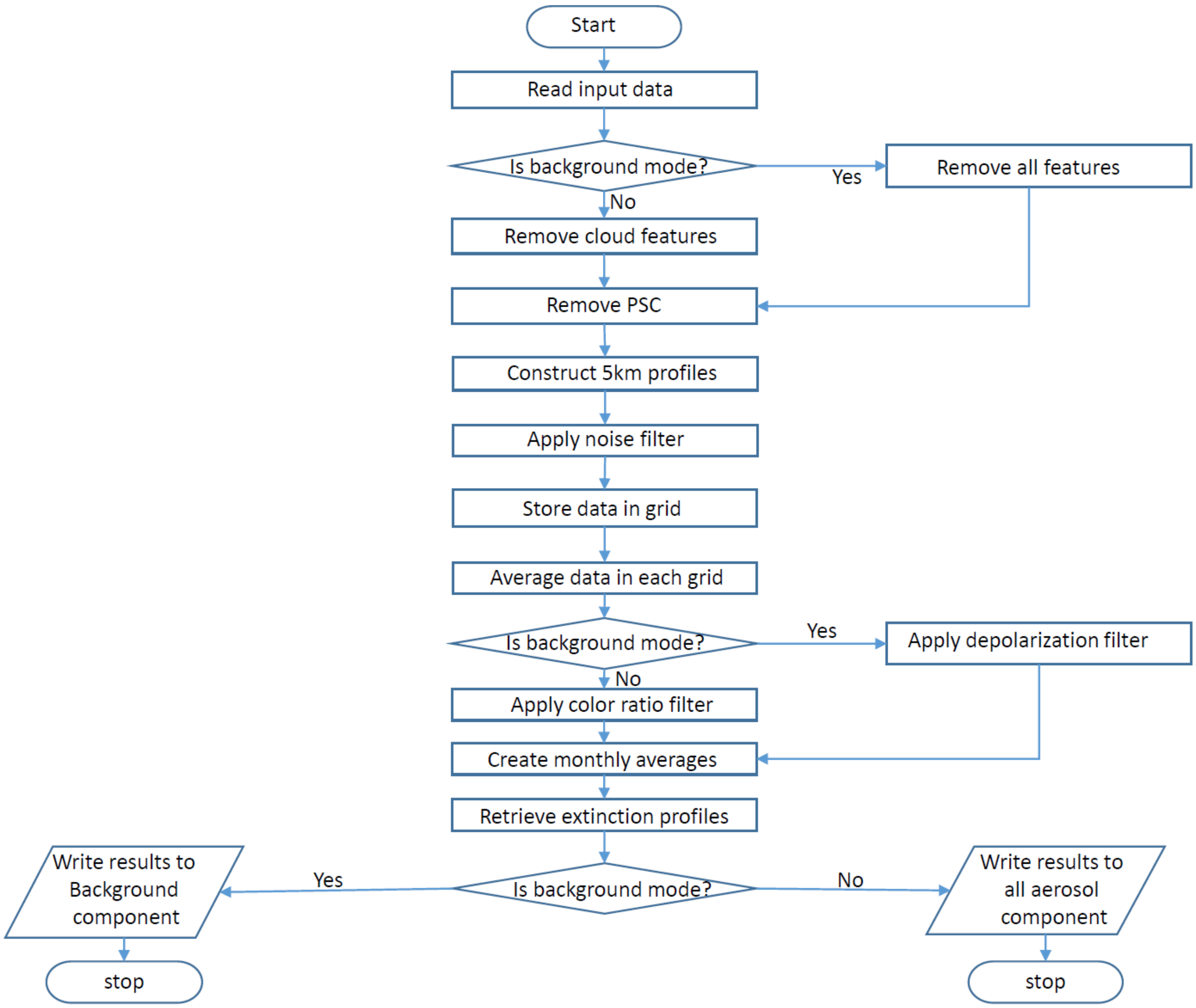

Figure 2. Overall design of the CALIPSO stratospheric aerosol product.

In the "background mode", clearing the features detected in the level 2 analyses is done by removing all the level 1B (L1B) attenuated backscatter values (for 15 consecutive L1B profiles) below the top of the uppermost cloud or aerosol layers detected above the local tropopause using the layer heights reported in the 5 km merged layer file. Not only are signals from within the boundary of the layers removed, the backscatter values at all altitudes below the layers are also removed to avoid issues in correcting for signal attenuation from overlying layers. While the attenuated backscattered signals within and below these layers are removed, this step will retain values which fall below the minimum detectable attenuated backscatter threshold of the CALIPSO layer detection algorithm (McGill et al., 2007). In this sense, the retrieved extinction in this mode will reflect only the aerosol loading below this threshold. Similarly, the signals below the uppermost PSC layers are also removed using the PSC mask file for the PSC-active months in the two hemispheres (December through March in the Arctic and May through October in the Antarctica) . The PSC mask files report the occurrence of PSCs in both the hemispheres (Pitts et al., 2007, 2009) and are reported for a single day on a 5 km horizontal and 180 m vertical grid for nighttime conditions only.

After clearing all level 2 and PSC layers detected above the local tropopause, all L1B attenuated backscatter values below the tropopause are removed. Further, all L1B profiles within the South Atlantic Anomaly (SAA) region are also removed. In this region, between approximately the equator and 50^{o}S in latitude and 20^{o}E to 80^{o}W in longitude (in the operational algorithm a polygon is used), the Van Allen belts come down to their lowest altitude (< 200 km), thus exposing the satellite sensors to high fluxes of energetic charged particles which are trapped within the belts (Hunt et al., 2009, Noel et al., 2014). Large amplitude noise excursions are often observed in attenuated backscatter profiles within this area, thus degrading the already low SNR in the stratosphere. Consequently, data over the SAA are not included when calculating the stratospheric aerosol product.

When creating the "all aerosol" mode of the stratospheric aerosol product, it is necessary to remove any clouds and PSCs, much the same way as for the background case, but retain the detected layers classified as aerosols by the CALIPSO cloud-aerosol discrimination (CAD) algorithm (Liu et al. 2009, 2019). It should be mentioned that the CAD algorithm was also modified in V4 in order to be compatible with the new V4 532 nm calibration (Liu et al., 2019). In fact, the CAD algorithm was extended to the stratosphere for the first time in V4. Up until V3, any layer in the stratosphere was simply classified as a "stratospheric feature" and no distinction was made between clouds and aerosols. However, even the V4 CAD algorithm may not perform very well at high altitudes because of low SNR leading to generally lower CAD scores (Liu et al., 2019). In any case, in the stratospheric altitudes above ~20 km, clouds are seldom observed (except in the polar regions) and uncertainties in the CAD algorithm are not likely to affect the stratospheric aerosol product. For this mode, only aerosol layers with acceptable CAD scores (-100 to -20) are retained within the stratosphere. Layers identified as aerosols but with unacceptably low CAD scores (between 0 and -20) are removed as if they were clouds or PSCs.

In the next step, a nominal 5 km resolution profile is constructed by taking the average of these 15 filtered L1B attenuated backscatter profiles. Subsequently, a noise filter is used to screen out strong outliers from these 5 km profiles that might otherwise lead to biases in high latitude and/or high altitude regions. The noise filter used for the current version of the product is a reconfigured version of the same filter that is used in the CALIPSO range dependent automated level 2 layer detection algorithm and includes contributions from both range-invariant and range-dependent noise sources (for details, see Vaughan et al., 2009, section 2c). After removing these outliers, the 5 km profile is assigned to the appropriate spatial grid. This process is then repeated for all the profiles in the level 1B file. The resulting filtered 5 km profiles are then averaged to create a single mean attenuated backscatter profile for each grid cell.

In the final processing step for each granule, another quality screening is employed to identify and remove any lingering tenuous cirrus cloud in the lower stratosphere that might have escaped the layer detection mechanism due to low backscatter values. For the "background" mode, we can safely assume the background aerosols are uniformly spherical and thus have a near zero depolarization ratio. Since ice crystals in even the most tenuous cirrus violate this assumption, we use a threshold of 5% in volume depolarization ratio (ratio of the attenuated backscatter measured in the perpendicular and parallel channels at 532 nm (Hunt et al., 2009)) to detect weakly scattering residual clouds (e.g., as described in Vernier et al., 2009). However, for the "all aerosol" mode, this strategy will not work. This is because volcanic ash is typically non-spherical and has high volume depolarization values (~25-30%) and thus would be removed along with the cirrus clouds. On the other hand, attenuated color ratio values (i.e., the ratio of the total attenuated backscatter coefficients at 1064 nm and 532 nm) are generally larger for clouds as compared to the volcanic ash and thus may be used to filter out clouds while still retaining volcanic ash (Winker et al., 2012; Vernier et al., 2014). The distribution of clouds and ash from the Puyehue-Cordon Caulle volcano (June 2011) at 17 km suggest that the two layer types can be discriminated reasonably well by using a threshold value of 0.5 in attenuated color ratio (Vernier et al., 2014). We therefore use this threshold in attenuated color ratio to retain the volcanic ash in the "all aerosol" mode, instead of the volume depolarization filter.

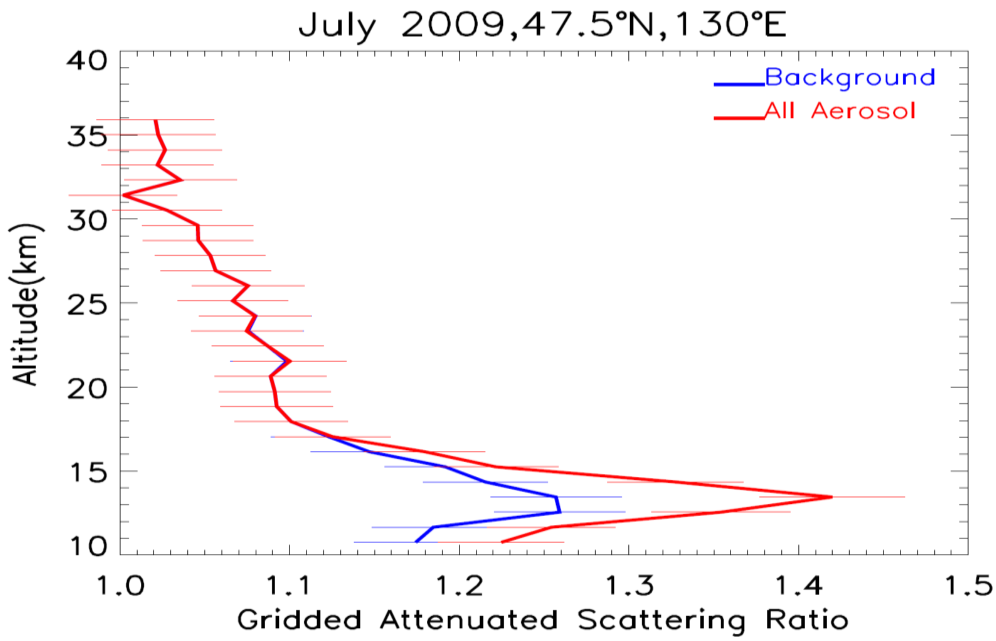

Figure 3. Profiles of attenuated scattering ratio at 47.5°N and 130°E in July 2009 for the background (blue) and all aerosol (red) components. The error bars represent computed uncertainties.

Figure 3 shows the profiles of attenuated scattering ratio for the background and all aerosol modes in July 2009 for the grid cell centered at 47.5°N and 130°E. The enhanced scattering ratio in the lower stratosphere between 10-km and 17-km is due to the inclusion of detected aerosol layers from the Sarychev volcano (48.1°N, 153.2°E), which erupted in June 2009. Note that backscatter from some of the Sarychev aerosols which fall below the minimum detectable backscatter threshold will contribute to the background profile.

After deriving the granule-averaged data, we create monthly averaged gridded profiles of attenuated backscatter by aggregating all profiles during each month of the mission. In addition to the attenuated backscatter coefficient profiles, profiles of molecular and ozone number densities, temperatures, and pressures reported in the L1B files are also averaged and gridded for use in the subsequent retrieval procedures.

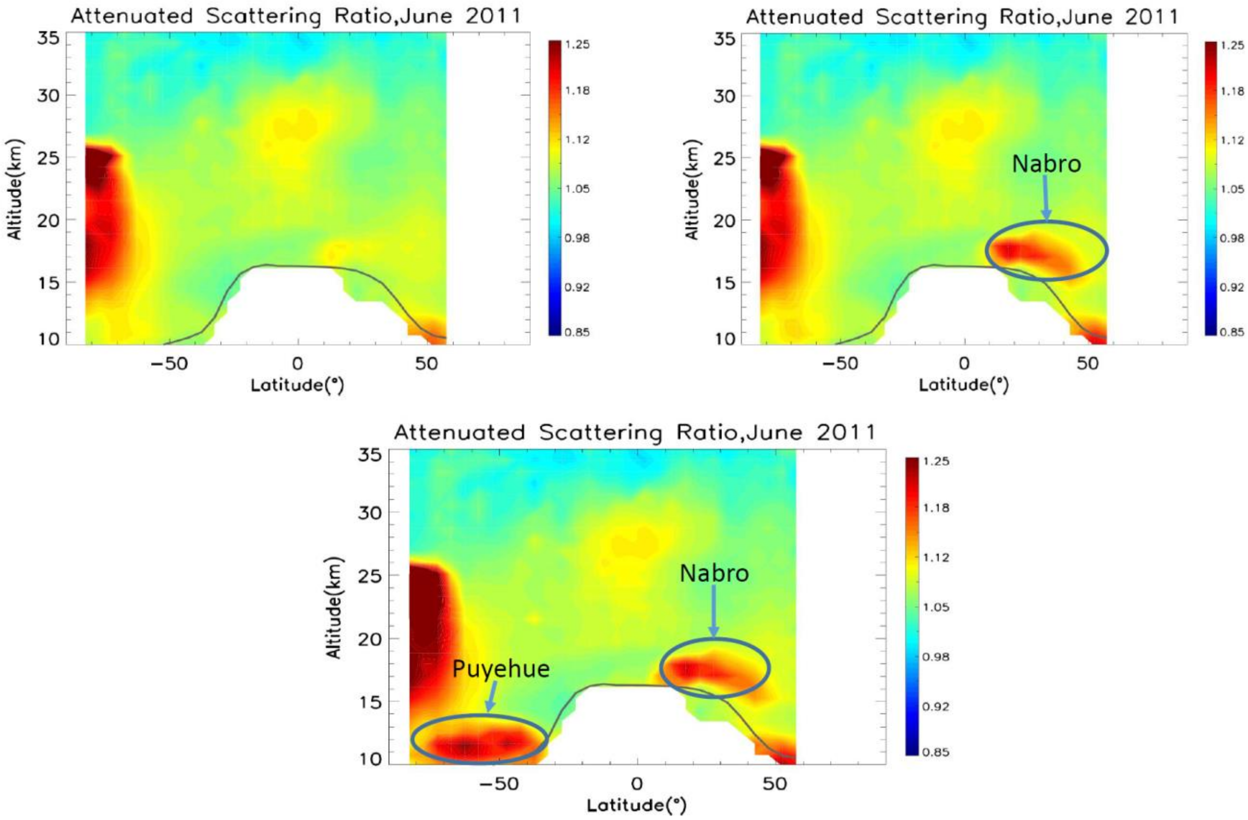

Figure 4. Zonally averaged height-latitude cross sections of attenuated scattering ratio for June 2011 a) after removing all detected layers and using a depolarization filter, b) including only aerosol layers in the stratosphere with a depolarization filter and c) including aerosol layers but using a color ratio filter.

Figure 4 shows the effect of different filters on the height-latitude cross sections of the gridded attenuated scattering ratio profiles for the month of June 2011. During this month two strong volcanic eruptions took place, Nabro in the northern hemisphere (June 13th, 13°N, 41°E) and Puyehue-Cordon Caulle in the southern hemisphere (June 4th, 40°S, 72°W). The composition of the Nabro plume was mostly sulfate while the composition of Puyehue-Cordon Caulle was mostly ash (de Vries et al., 2014; Vernier et al., 2013). In the background mode (Figure 4a), removal of all detected layers combined with the application of the depolarization filter ensures that stratospheric perturbations from these two volcanoes are mostly excluded. Figure 4b shows the effect of including aerosol layers in the stratosphere with acceptable CAD scores (|CAD| > 20) while still using the depolarization filter. Now the Nabro plume can be clearly seen but not that of Puyehue-Cordon Caulle. This is because the sulfates in the Nabro plume have low depolarization ratios that fall below the threshold and are thus retained while the ash layers with high depolarization ratio from Puyehue-Cordon Caulle are removed. On the other hand, inclusion of the aerosol layers when using a color ratio threshold of 0.5 in Figure 4c (all aerosol mode) reveals both the Nabro and Puyehue-Cordon Caulle plumes (near 50°S) quite clearly. Note the high scattering ratio values in the Antarctic latitudes between 15-km and 25-km. Since all PSC layers detected by the PSC mask product were removed, these are probably signatures of particles in the process of becoming PSCs.

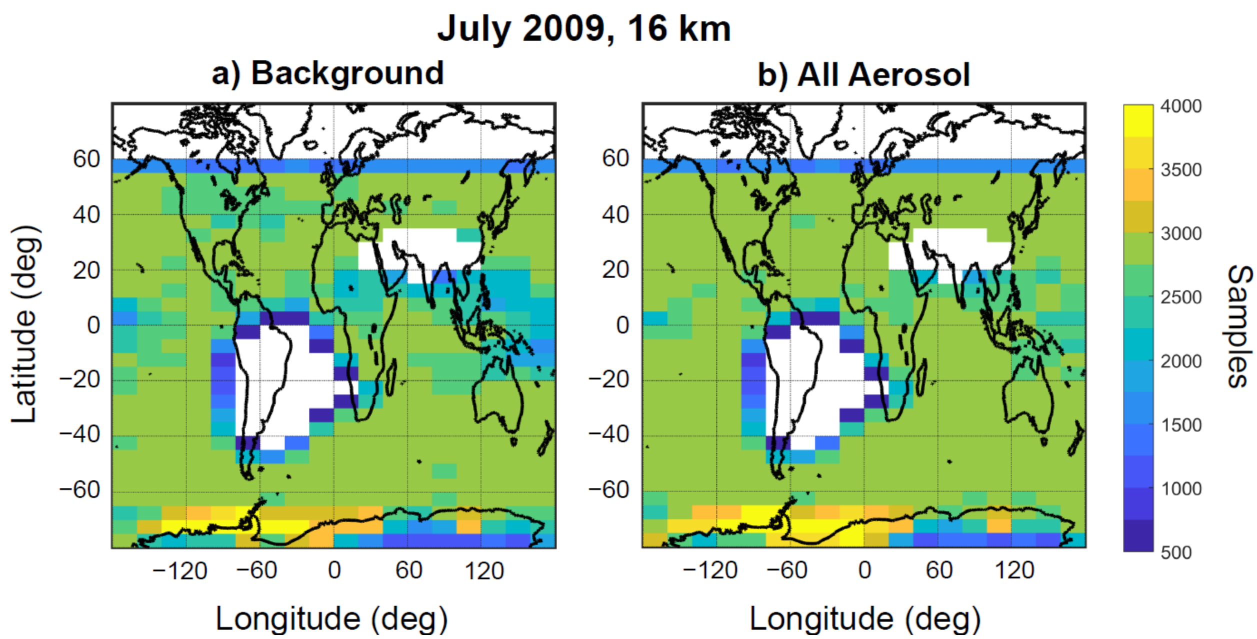

Figure 5. Number of samples contributing to a) background mode and b) all aerosol mode at 16 km in July 2009. Grid cells with < 50 samples are plotted in white.

Figure 5 depicts the spatial distribution of the number of samples that contributed to the two components at 16 km during July 2009. The white grid cells over South America and parts of South Atlantic Ocean correspond to the SAA, over which all data samples are rejected. The white grid cells over southeast Asia occur because the tropopause is higher than 16 km in this region. Higher numbers of samples for the all aerosol mode over the surrounding area might be related to the influence of deep convection during the monsoon period. Higher numbers of samples in the all aerosol mode can also be seen over North America, which is likely related to the Sarychev volcano as mentioned above. Also note the high number of samples over parts of Antarctica. This is again likely due to small particles which are in the process forming PSCs.

2.2.2 Retrieval of aerosol extinction profiles

The monthly mean profiles of gridded 532 nm attenuated backscatter coefficient (β'), constructed using the procedure described in the preceding section, along with gridded profiles of molecular backscatter coefficients (β_m), molecular extinction coefficients (α_m), and ozone absorption coefficients (α_{O_3}), are used to retrieve the particulate backscatter coefficient (β_p) using

$$\beta_p(r) = \beta'(r) / T^2_m\, T^2_{O3}\, T^2_p - \beta_m(r) \quad (2)$$

where,

$$T^2_m(r) = \exp\left(-2 \int_0^r \alpha_m(r')\, dr'\right), \quad (3a)$$

$$T^2_{O_3}(r) = \exp\left(-2 \int_0^r \alpha_{O_3}(r')\, dr'\right), \text{ and} \quad (3b)$$

$$T^2_p(r) = \exp\left(-2\, \eta_p\, S_p \int_0^r \beta_p(r')\, dr'\right). \quad (3c)$$

In these expressions, η_p is the particulate multiple scattering factor, S_p is the particulate lidar ratio (i.e., the extinction-to-backscatter coefficient ratio), and T^2_m, $T^2_{O_3}$, and T^2_p are, as previously defined, the molecular, ozone, and particulate two-way transmittances. The molecular backscatter coefficients and molecular and ozone two-way transmittances can be calculated from molecular model data (e.g., as described in Kar et al., 2018). The molecular model used exclusively throughout the CALIPSO V4 data products is the Modern-Era Retrospective analysis for Research and Applications 2 (MERRA-2) provided by NASA's Global Modeling and Assimilation Office (Gelaro et al., 2017). For the CALIPSO stratospheric aerosol product, the particulate multiple scattering factor is taken as 1 for all species of stratospheric aerosols.

Given an appropriate value of the lidar ratio, equations 2 and 3c can be solved iteratively to obtain estimates of $\beta_p(r)$ (Young and Vaughan, 2009). Estimates of particulate extinction coefficients are subsequently obtained using $\alpha_p(r) = S_p \times \beta_p(r)$. The V1.00 release of the level 3 stratospheric aerosol product uses a value of S_p = 50 sr for the stratospheric aerosol lidar ratio, which is a typical value used for stratospheric aerosols for background conditions and in absence of significant ash injections from volcanoes (Trickle et al., 2013, Ridley et al., 2014, Sakai et al., 2016, Kremser et al., 2016, Khaykin et al., 2017). We also assume S_p to be constant at all latitudes and over the entire altitude range. To guarantee uniform results across multiple CALIPSO data product levels, the level 2 CALIPSO extinction retrieval module is used to calculate the level 3 profiles of stratospheric aerosol extinction and backscatter coefficients and their uncertainties. The details of the retrieval process and uncertainty estimates are given in Young and Vaughan (2009) and Young et al. (2013, 2016, 2018) and are not repeated here.

3. Initial assessment of CALIPSO stratospheric aerosol product

In this section we assess the initial performance of the CALIPSO stratospheric aerosol product by first presenting the signatures of various stratospheric aerosol events as captured by the product and then making quantitative comparisons with observations from SAGE III on ISS.

3.1. Signatures of stratospheric events and dynamics.

3.1.1 Effects of volcanic and smoke injections.

Volcanoes are one of the primary sources of stratospheric aerosols (e.g. Kremser et al., 2016). Ground based lidar studies have indicated a rising trend in the stratospheric sulfate aerosol loading since the turn of the century which was initially attributed to anthropogenic emissions of SO_2 from coal burning in South East Asia (Hofmann et al., 2009). However, closer scrutiny suggests that the increase is instead related to emissions of SO_2 from a large number of moderate volcanic eruptions, as was initially suggested by Vernier et al. (2011) based on analyses of CALIPSO data. Several volcanoes with stratospheric impacts have been recorded since the study by Vernier et al. (2011). Volcanic signatures in CALIPSO data were examined more recently by Friberg et al. (2018).

Figure 6 shows the time-altitude cross section of the zonally averaged extinction coefficients between 25^{o}S to 25^{o}N from the CALIPSO level 3 stratospheric aerosol product between January 2007 and December 2017. The signatures of many volcanoes are clearly evident in this image. While some of the volcanoes injected material only in the lower stratosphere (Kasatochi, Nabro etc.), the influence of some other volcanoes reached significantly higher, in particular Kelud in 2014.

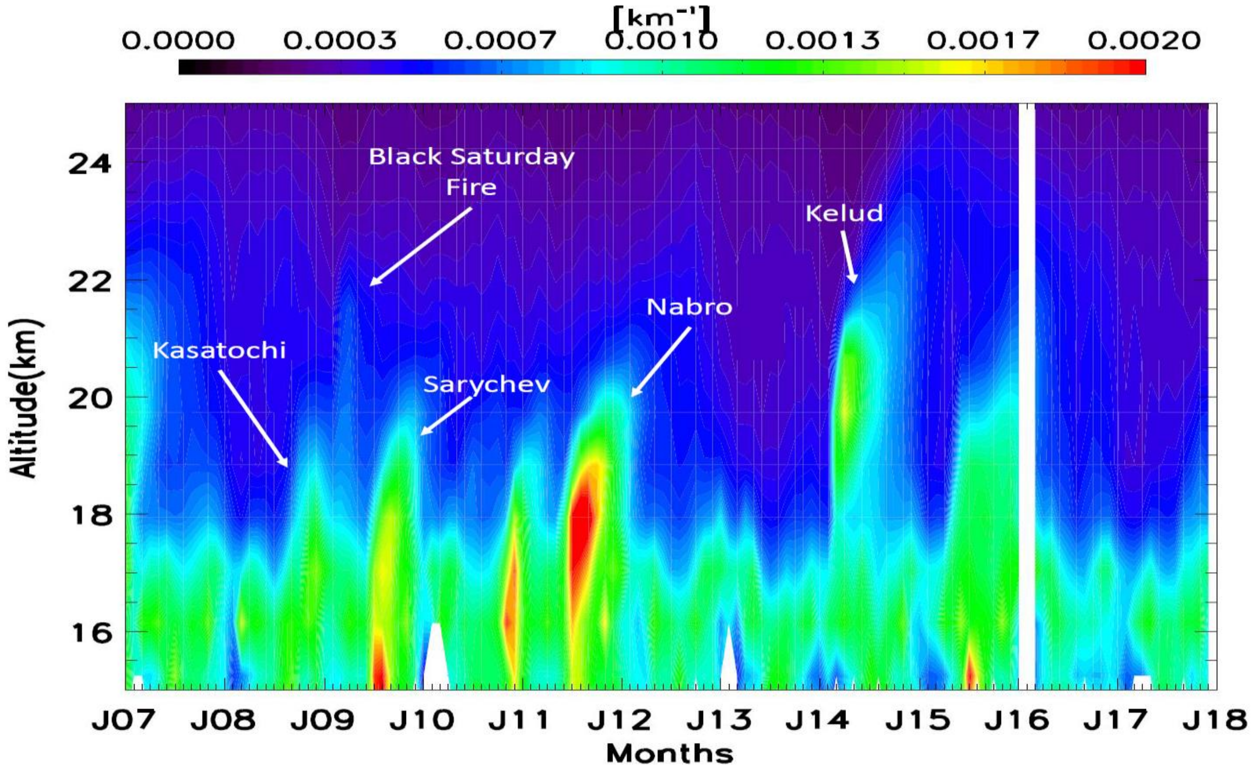

Figure 6. Time-altitude cross section of the retrieved extinction coefficients, averaged between 25°S to 25°N, from January 2007 through December 2017.

Apart from volcanic material, smoke from strong biomass burning events can also reach the stratosphere during the so-called pyrocumulonimbus events (Fromm et al., 2010; Peterson et al., 2018). During the “Black Saturday” event, smoke from strong bushfires in Victoria, Australia on February 7, 2009 is known to have impacted the stratosphere. Plumes from this blaze eventually reached altitudes of 16–20 km and were readily visible in satellite imagery (de Laat et al., 2012; Glatthor et al., 2013). The signature of this event can also be quite clearly seen in Figure 6. These pyrocumulonimbus events seem to be increasing in frequency and currently there is a strong research focus on them (Peterson et al., 2018).

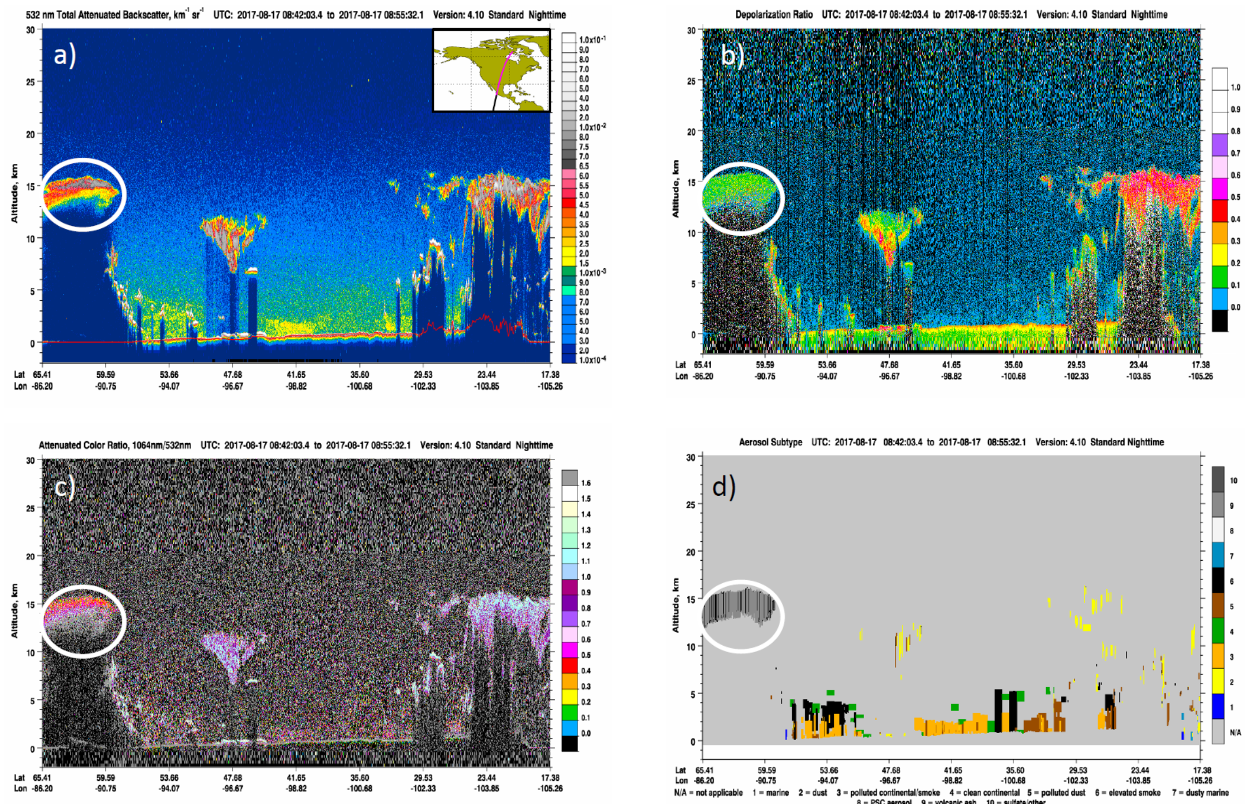

Figure 7. CALIPSO browse images of a) 532 nm total attenuated backscatter, b) 532 nm volume depolarization ratio, c) attenuated backscatter color ratio (1064 nm / 532 nm) and d) aerosol subtypes of a pyroCb event over Canada on August 17, 2017. The smoke plume is shown in the white circles.

The extreme pyroCb event that occurred in August 2017 over British Columbia in Canada has been extensively studied recently and has been likened to volcanic perturbations in the stratosphere in terms of intensity and duration (Khaykin et al., 2018; Ansmann et al., 2018; Haarig et al., 2018, Peterson et al., 2018). Figure 7 shows an example of the CALIPSO measurements of this pyroCb event. The signature of the smoke plume is seen as extremely high attenuated backscatter (opaque at 532 nm) between 60^{o}N and 65^{o}N. The very high attenuated color ratio (~1.6) seen at the base of the plume (Figure 7c) is a tell-tale signature of smoke (e.g. Liu et al., 2008). The high volume depolarization ratio ($\geq$ 0.1) seen in Figure 7b is unusual for smoke and suggests the presence of irregular soot particles and mineral dust, with fast adiabatic lifting possibly retaining the initial irregular shapes (Haarig et al., 2018, Khaykin et al., 2018). This high color ratio combined with the unusually high depolarization results in the plume being identified as a mixture of smoke and "volcanic ash" (Figure 7d), the latter being misclassifications by the CALIOP V4 level 2 scene classifier.

Figure 8 shows the height-latitude cross sections of CALIOP attenuated scattering ratios from the stratospheric aerosol product between August 2017 and November 2017 and captures the evolution of the aforesaid pyroCb event. After the original injection of smoke in August 2017 at mid-latitudes, the smoke spreads globally and to lower latitudes as can be seen in these monthly mean spatial distributions from the level 3 stratospheric aerosol product.

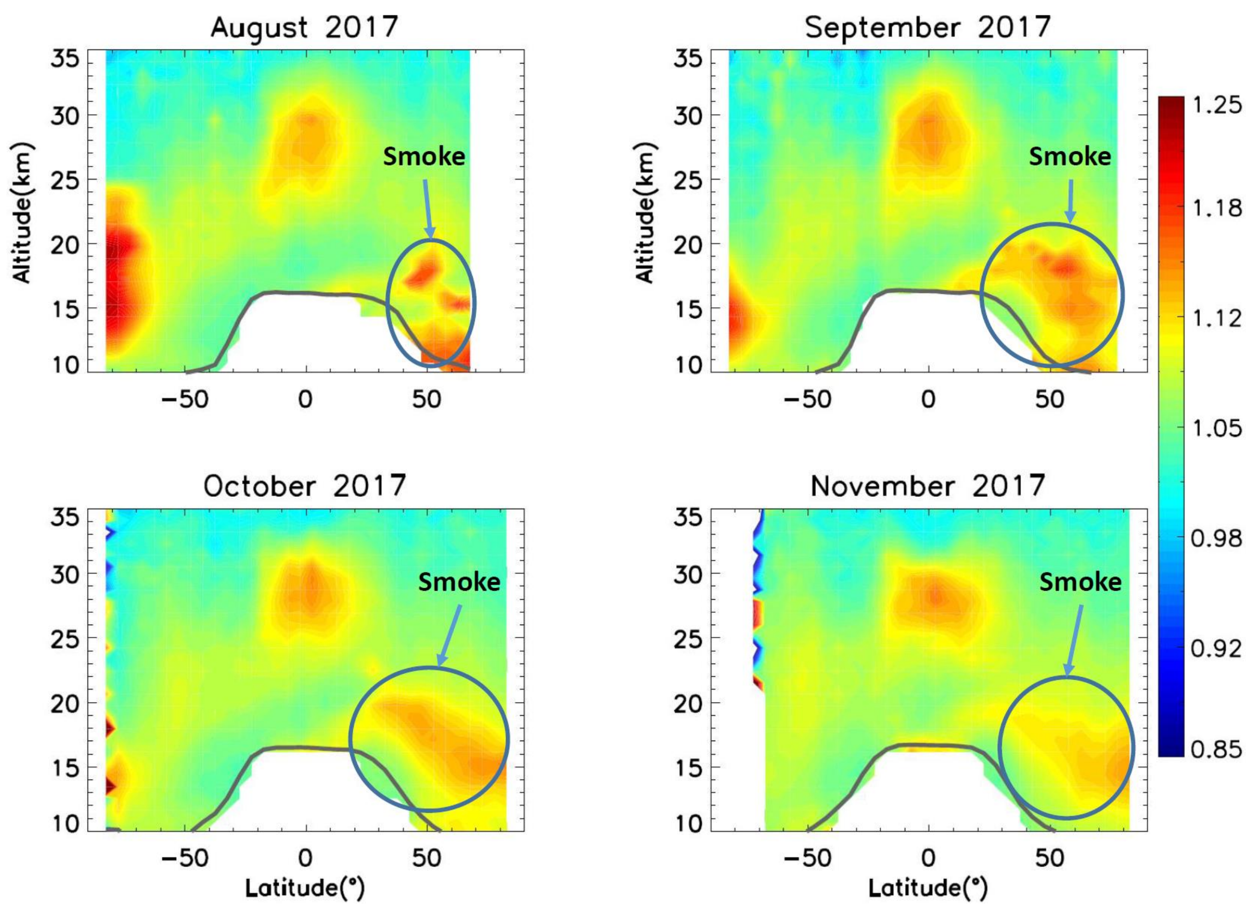

Figure 8. Zonally averaged height-latitude cross section of the 532 nm attenuated scattering ratios from August 2017 through November 2017.

3.1.2. Signatures of stratospheric dynamics

Figure 9 shows the height-latitude cross section of the retrieved 532 nm extinction coefficients for the "all aerosol" mode from February to October 2014, which captures the evolution of the Kelud (April 2014, 7.9^{o}S, 112.3^{o}E) eruption in altitude. The gradual lofting of the plume from around 17 km over the tropics to nearly 24 km over several months shows the signature of stratospheric dynamics in the CALIPSO stratospheric aerosol product The persistence of the stratospheric perturbation for several months is consistent with the results of Vernier et al. (2016) who found the presence of ash in the lower stratosphere 3 months after the Kelud eruption from balloon observations.

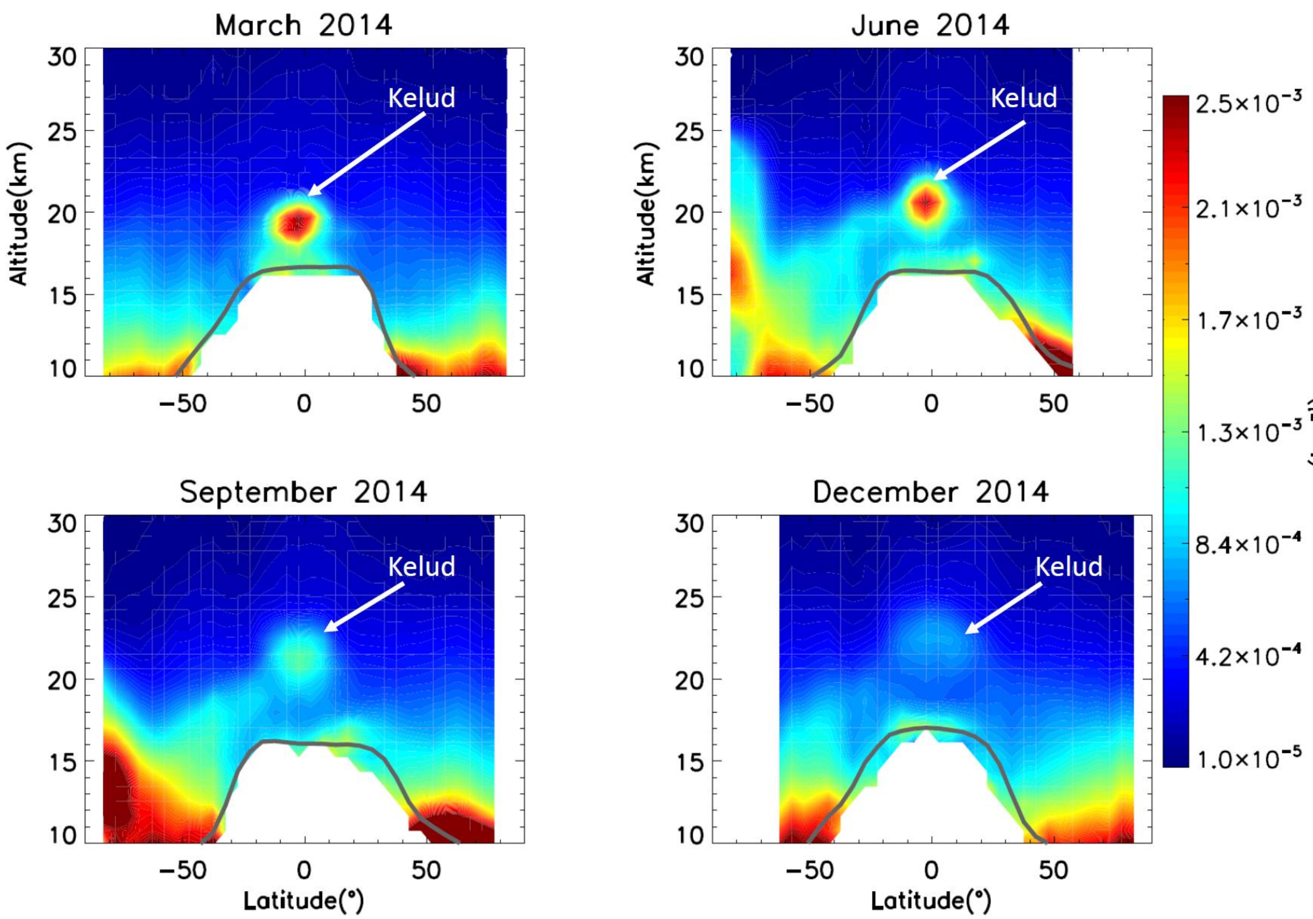

Figure 9. Zonally averaged height-latitude cross sections of 532 nm extinction coefficients (km^{-1}) in March, June, September and December of 2014.

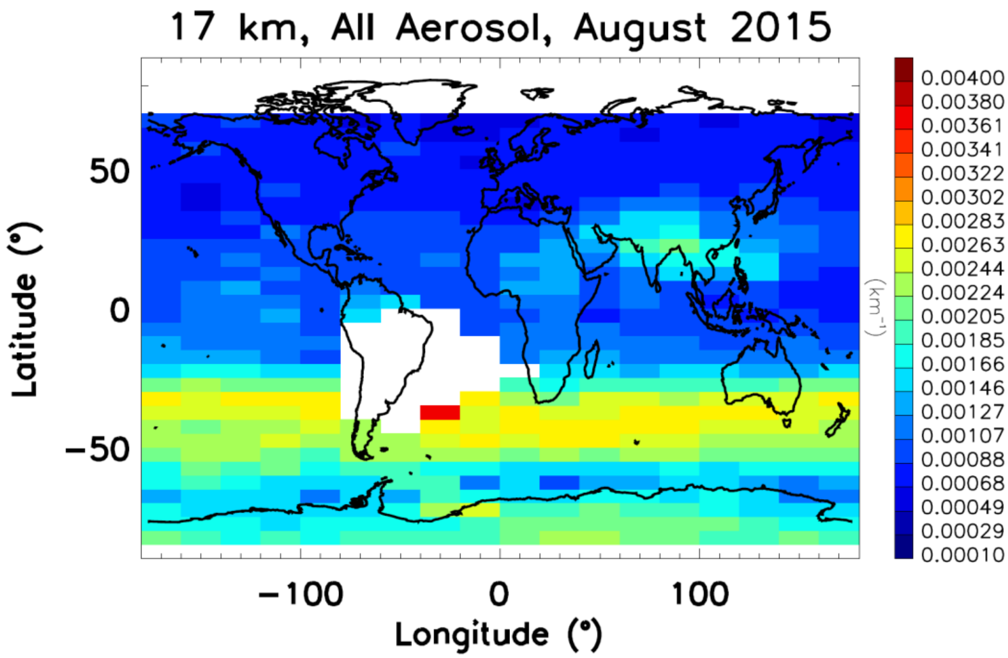

Figure 10. Retrieved 532 nm extinction coefficients (km^{-1}) at 17 km for August 2015.

Figure 10 shows the spatial distribution of the retrieved extinction coefficients at 17 km for the month of August 2015 for the “all aerosol” mode. Two strong perturbations of the lower stratosphere can be seen in this plot. The first is the plume from the Calbuco volcano in Chile which erupted in April 2015 and spread around the southern hemisphere in a belt between 60°S to 30°S (Lopes et al., 2019). The other is the plume of high extinction over southeast Asia and extending to the Arabian peninsula to the west. This is the location of the Asian summer monsoon anticyclone which has been known to be a reservoir of pollution during the monsoon months and results from deep convective outflow of pollutants both gases and aerosols from the surface layers (Kar et al., 2004, Vernier et al., 2011).

3.2. Comparison with SAGE III on ISS

In this section we provide an initial quantitative assessment of the CALIPSO level 3 stratospheric aerosol product by inter-comparison of the retrieved extinction coefficients with those from the SAGE III instrument aboard ISS. The SAGE III instrument was launched in February 2017 and has been providing measurements of ozone, NO_2, water vapor, and aerosols from its mount on the exterior of the ISS since March 2017 (Cisewski et al., 2014). The instrument derives its legacy from the long line of SAGE instruments which have been providing the most accurate retrievals of aerosol extinction in the stratosphere since 1984 (Chu et al., 1993; Thomason et al., 2008, 2010, Damadeo et al., 2013). SAGE III performs solar and lunar occultation measurements as the ISS orbits the Earth and covers the entire global latitude (90^{o}S to 90^{o}N) and longitude range (180^{o}W to 180^{o}E). The aerosol extinction profiles are available from the solar occultation measurements in 9 channels from 384 nm to 1544 nm. We use the latest version 5.1 extinction profiles reported in the 521 nm channel, which is the closest to the CALIPSO 532 nm channel. In order to compare with the CALIPSO level 3 product, which reports gridded monthly averages, we average the daily data from SAGE III onto the same latitude grid (zonally averaged) as CALIPSO over a month and interpolate to the CALIPSO altitude grid. Data from both the sunrise and sunset occultations are used in the comparisons. Further, the data were filtered for cloud contamination by selecting only those data having a 521 nm to 1022 nm extinction ratio greater than 2 (Thomason and Vernier, 2013). We convert the SAGE III data at 521 nm to 532 nm by using an Angstrom exponent (binned into 5° latitude bins and interpolated to CALIPSO altitude grid) derived from the extinctions retrieved at 521 nm and 1022 nm by SAGE III for the same month. Measurements from both the instruments from June 2017 through August 2018 were used for this comparison. The globally averaged value of the Angstrom exponent derived using all 15 months of data is about 1.56, essentially same as the constant value used by Khaykin et al. (2017) to convert SAGE II extinctions at 525 nm to 532 nm. We used only extinction values with corresponding fractional extinction uncertainty less than 100% for retrievals from both the instruments and calculate the differences between CALIPSO and SAGE III from the following equation:

$$\Delta (z) = 100\times(\sigma (z)_{\mathrm{CALIPSO}} - \sigma (z)_{\mathrm{SAGE}})/\sigma (z)_{\mathrm{SAGE}} \qquad (4)$$

where $\sigma(z)_{\mathrm{CALIPSO}}$ is the extinction coefficient at altitude z from CALIPSO and $\sigma(z)_{\mathrm{SAGE}}$ is the extinction coefficient SAGE III at the same altitude. Further, we use zonally averaged (into 5° latitude bins) profiles for height resolved comparisons and only the “all aerosol” mode from CALIPSO product for the sake of compatibility.

a)

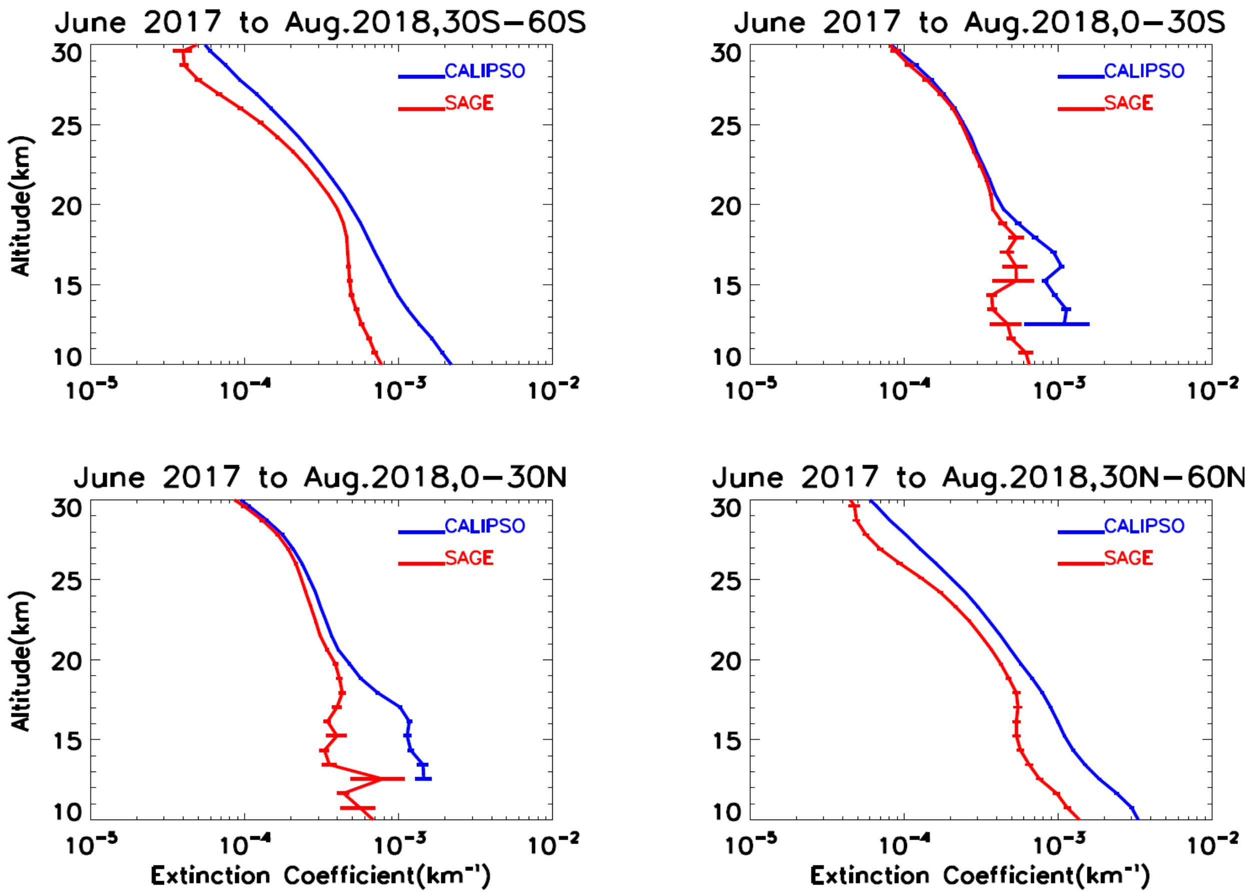

June 2017 to Aug.2018,30S−60S
June 2017 to Aug.2018,0−30S
June 2017 to Aug.2018,0−30N
June 2017 to Aug.2018,30N−60N
CALIPSO
SAGE
Altitude(km)
Extinction Coefficient(km⁻¹)

b)

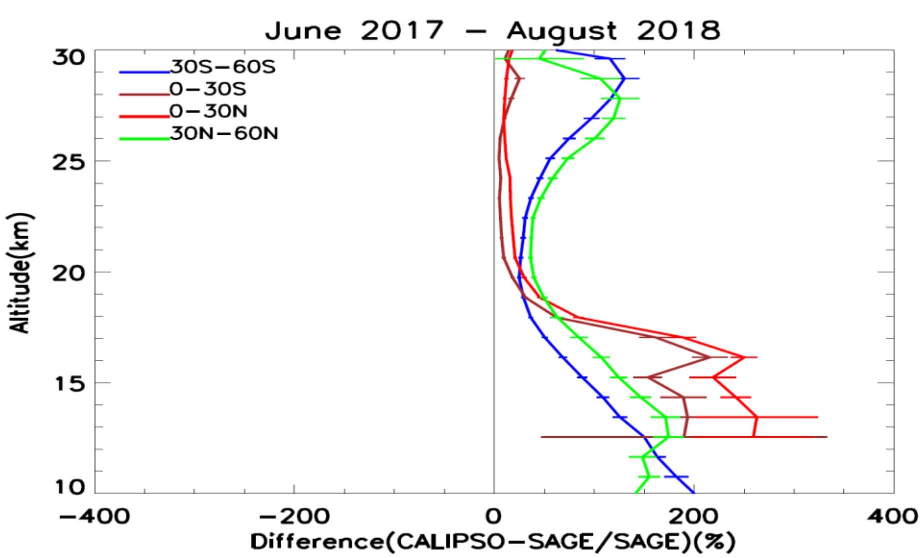

June 2017 − August 2018
30S−60S
0−30S
0−30N
30N−60N
Altitude(km)
Difference(CALIPSO−SAGE/SAGE)(%)

Figure 11 a) Altitude-resolved profiles of the mean 532 nm extinction coefficient retrieved from CALIPSO and SAGE III on ISS using all available data between June 2017 and August 2018. The corresponding average differences are shown in panel b). The differences are calculated at each latitude and altitude grid for each month and then the average is taken over all the available months. The error bars represent the standard errors of the mean.

Figure 11a shows zonally averaged mean profiles of extinction coefficients retrieved from CALIPSO (in blue) and SAGE III (in red) at 4 latitude bands using the same 15 months of measurements from the two instruments. Figure 11b shows the profiles of the fractional differences in the same latitude bands. The profiles for 0-30^{o}S and 0-30^{o}N, generally show fairly good agreement with the average difference within about 25% between 20 km and 30 km. The comparisons for 30^{o}S-60^{o}S and 30^{o}N-60^{o}N are similar and both show significant differences between CALIPSO and SAGE III extinction at all altitudes with CALIPSO having a high bias. All the profiles diverge significantly at altitudes below 20 km, with the average difference often exceeding 100% and CALIPSO consistently overestimating SAGE III. Note that the aerosol retrievals from SAGE III (as for the legacy retrievals from SAGE II) are not directly filtered for the presence of clouds which may impact the retrievals in the lower stratosphere. Thomason and Vernier (2013) discussed this issue in respect of SAGE II data. As these authors have pointed out, this is a difficult task and it is not always to possible to completely remove the cloud effects. Following their analysis we have attempted to remove the cloud contamination in the extinction retrievals by using only those data for which the ratio of extinctions at 521 nm and 1022 nm is greater than 2.0. SAGE III aerosol extinctions have not been validated as of now and it is not clear if there are any issues with the retrievals at lower altitudes near the tropopause.

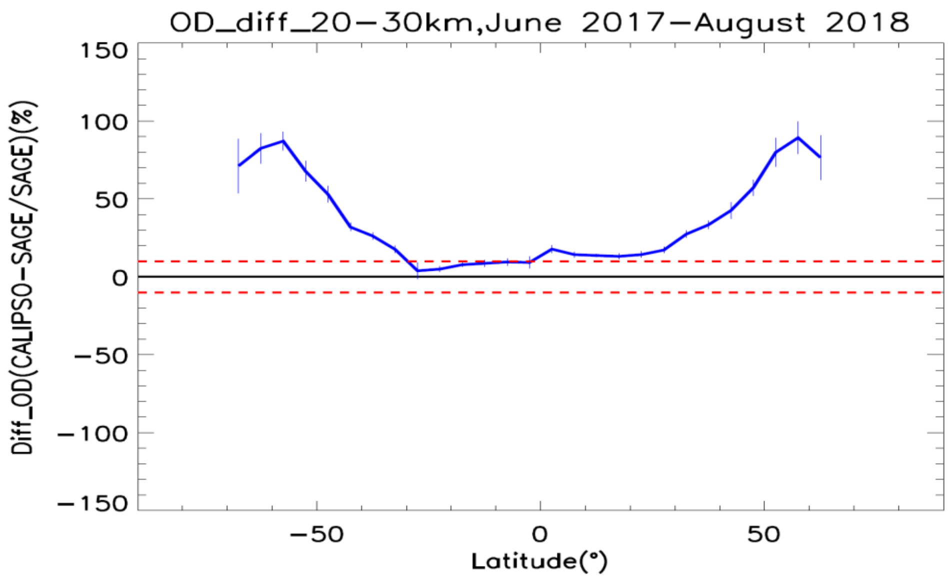

Figure 12. Fractional difference in 532 nm optical depth between CALIPSO and SAGE III calculated using extinction coefficients from 20-30 km, as a function of latitude. The dashed red lines demarcate the ±10% difference levels. The error bars represent the standard error of the mean.

Figure 12 shows the difference in the stratospheric optical depths between CALIPSO and SAGE III, calculated using the average extinction coefficient profiles between 20 km and 30 km. This region is not likely to be affected significantly by clouds and also is the region where most of the stratospheric aerosol resides, thus comparisons here are likely to be indicative of the overall performance differences between the two sensors. Between 30°S to 30°N the optical depths are in agreement to within about 10-20%, though the differences begin to rise substantially in the mid-latitudes of both hemispheres.

4. Discussion:

For an initial assessment of the CALIPSO stratospheric aerosol product, we have used the aerosol retrievals from SAGE III on ISS acquired between June 2017 and August 2018. The solar occultation technique used for SAGE III retrievals does not rely on any assumptions on the aerosol size distribution. Further the retrieval wavelengths from SAGE III (521 nm) and CALIPSO (532 nm) are quite close and thus the comparison of the extinction retrievals will not be impacted significantly by errors in the Angstrom exponent. The previous section demonstrated that the retrieved aerosol extinction coefficients reported by the CALIPSO level 3 stratospheric aerosol product agree well with those reported by SAGE III between 20 km and 30 km within tropical latitudes, though the disparities between the two sets of measurements are significantly larger at higher latitudes. The primary parameter affecting the comparison with SAGE III is likely to be the lidar ratio used in the CALIPSO retrieval. The CALIPSO extinction retrievals are quite sensitive to the lidar ratio used in the retrieval algorithm (Young et al., 2013, 2016), and the lidar ratio depends upon the optical and physical properties of the scattering particles. In the troposphere, a look-up table of lidar ratios is used by the CALIPSO extinction retrievals for various types of aerosols that might be encountered, such as dust, smoke, marine aerosols etc. (Omar et al., 2009, Kim et al, 2018). The version 1.00 level 3 stratospheric aerosol product uses a constant lidar ratio of 50 sr at all latitudes and altitudes for the stratospheric aerosol retrievals. While a lidar ratio of 50 sr has frequently been adopted for stratospheric analyses (e.g. Trickle et al., 2013, Ridley et al., 2014, Sakai et al., 2016, Khaykin et al., 2017), it is not clear if this value is valid all over the stratosphere.

The adopted lidar ratio for the CALIOP stratospheric aerosol retrievals can be assessed by using the independent extinction retrievals from SAGE III and the attenuated backscatter measurements from CALIOP. For this we rewrite the Eq. (3c) as

$$T^2_p = \exp\left(-2 \int_0^r \sigma_p(r')dr'\right), \quad (5)$$

where $\sigma_p(r)$ is the particulate extinction coefficient as retrieved from the occultation measurements from SAGE III. Using these two-way transmittances from aerosols and computing all other terms in Eq. (2) and Eq. (3) from CALIOP data as earlier, we can obtain an estimate of the particulate backscatter $\beta_p(r)$. The range dependent lidar ratio $S_p(r)$ may then be obtained from the expression:

$$S_p(r) = \sigma_p(r) / \beta_p(r) \quad (6)$$

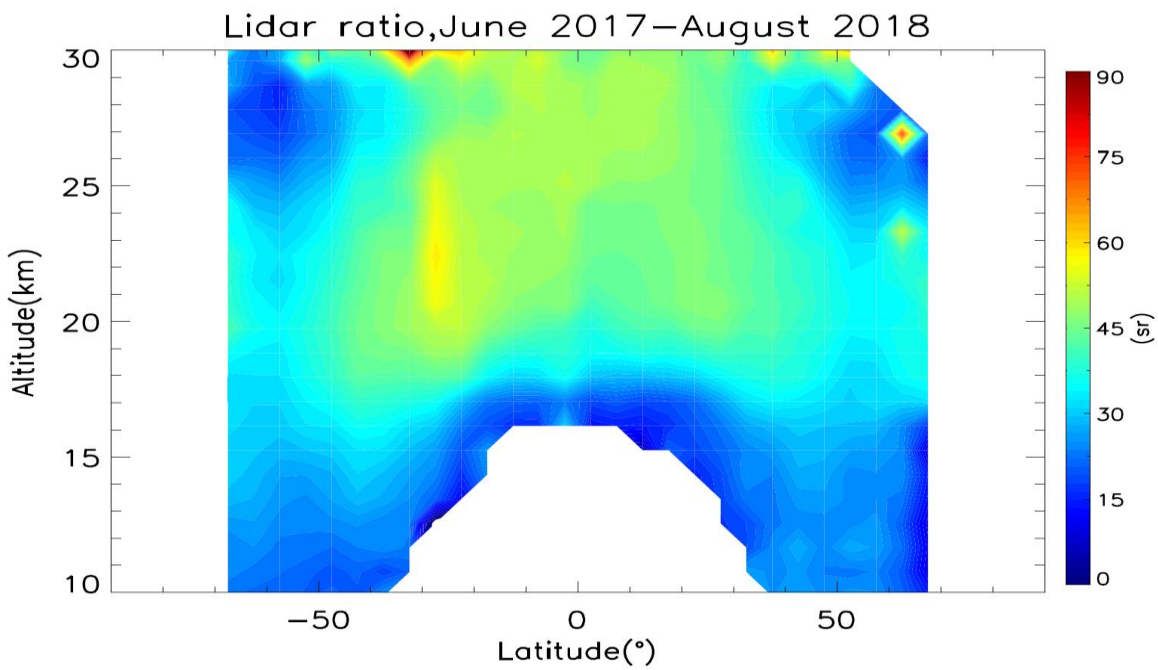

Figure 13. Spatial distribution of the stratospheric aerosol 532 nm lidar ratio obtained from the extinction retrievals from SAGE III and backscatter measurements from CALIOP.

Figure 13 shows the height-latitude cross section (averaged over June 2017-August 2018) of the estimated lidar ratios from the SAGE III and CALIOP measurements. As for the comparisons presented in section 3, we have cloud cleared the SAGE III data below 20 km by only using the 521 nm extinction coefficients when the ratio of extinctions at 521 nm and 1022 nm exceeded 2 and used an Angstrom exponent obtained from these two wavelengths to convert the extinction at 521 nm to that at 532 nm. As can be seen, the lidar ratio values in the bulk of the stratosphere with significant aerosol loading are in the range 45-50 sr, quite similar to the canonical range in the stratosphere (Kremser et al., 2016), with the mean value between 18-30 km and between 40^{o}S and 40^{o}N being ~46 ± 5 sr. However, in the lowermost stratosphere at all latitudes and in the both the polar regions at essentially all altitudes, the estimated lidar ratio values are substantially lower (Figure 13). There may be several issues impacting these estimated lidar ratios. We have used the 521 nm aerosol extinction product from SAGE III, which is still an evolving product. In particular, any errors in the ozone retrievals from SAGE III are likely to adversely affect the 521 nm aerosol extinction retrievals. Further, in the lowermost stratosphere above the tropopause, mixtures of clouds and aerosols may exist and SAGE III aerosol data have not been cleared for clouds as such. We have used a simple cloud clearance procedure using the ratio of extinctions at 521 nm and 1022 nm, which might be of limited validity near the tropopause. Similarly, at high altitudes in the polar regions the aerosol loading is expected to be quite small (extinction ~ 10^{-5} km^{-1}) and both sensors are likely to experience difficulty in retrieving these very low extinction coefficients. In particular, CALIOP can have significantly enhanced noise at those altitudes in the polar regions (e.g., see Fig. 16 in Hunt et al., 2009) which may contribute to the differences. Note also that a lidar ratio that is in error at the highest altitudes would lead to incorrect extinctions retrievals for CALIOP lower down, since the attenuation correction would be in error. In any case, using a lower lidar ratio in these areas as suggested by Figure 13, will lead to lower retrieved extinction coefficients from CALIOP and will alleviate the differences noted in section 3.

Is there any evidence of low lidar ratios in the high latitude stratosphere as seen in Figure 13? O'Neill et al. (2012) studied aerosol plumes from Sarychev volcano from high arctic observations from the Polar Environmental Atmospheric Research Laboratory (PEARL) station (80.05°N, 86.42°W) and estimated lidar ratio of 59 sr using size distribution from AERONET which was also close to the average lidar ratio of 55 sr estimated from the Arctic High Spectral Resolution (AHSRL) lidar between ~ 10-15 km. Kravitz et al. (2011) also reported lidar ratio of 50 sr and 60 sr for Sarychev plumes from the Koldewey Aerosol Raman Lidar (KARL) at Ny-Alesund, Svalbard (78.9°N, 11.9°W). Hoffmann et al. (2010) estimated a somewhat higher value of 65 sr for Kasatochi aerosol plume near the tropopause over Ny-Alesund, in September 2008. Interestingly, for a clear day with no Kasatochi layers, they obtained a background lidar ratio of 18 ± 6 sr by fitting the integrated lidar extinction to coincident photometer optical depth measurements. At high altitudes (> 20 km) in polar regions during non-PSC conditions, volcanic influence is not likely to be significant, however more data may be needed to verify the low lidar ratios at those altitudes. There is also a paucity of measurements at the stratospheric altitudes over the southern high latitude regions.

In presence of large ash and even sulfate injections from volcanoes, the lidar ratio can be significantly different and can evolve with time. From the so-called "constrained" retrievals, when the lidar ratios of layers can be obtained directly from the attenuation measurements from CALIOP (Young and Vaughan, 2009), the median lidar ratio of sulfate as well as ash-dominant layers from several volcanoes has been found to be ~ 60-69 sr (Prata et al., 2017, Kar et al., 2018). We have not filtered the data for the presence of volcanic and smoke particles, which can skew the lidar ratio estimates shown in Figure 13. For the data used here (June 2017 through August 2018), there were probably no significant injections of ash from volcanoes; however the large pyroCb event of August 2017 (as mentioned above) would contribute. In future versions of the CALIOP level 3 stratospheric aerosol product we shall attempt to use a more representative lidar ratio over all of the stratosphere.

5. Conclusion

In this paper we have provided a detailed account of the algorithm used to construct the CALIPSO level 3 stratospheric aerosol product version 1.00 that was recently released. Further, we have given qualitative as well as an initial quantitative assessment of the aerosol extinction retrievals. We have shown that the product captures significant stratospheric aerosol injections (e.g., from volcanic eruptions) and clearly illustrates perturbations from stratospheric dynamics over the lifetime of the mission. Comparisons with extinction retrievals obtained from SAGE III on ISS show quite good agreement to within about 25% in the mean between 20-30 km and between about 30^{o}S-30^{o}N. However the comparison consistently indicates much larger deviations, exceeding 100-200% (CALIPSO higher), at mid-to-high latitudes and high altitudes. The role of the lidar ratio used for the extinction retrievals in the level 3 stratospheric aerosol product was also explored. Based on combined measurements by CALIPSO and SAGE III, the current lidar ratio of 50 sr is shown to be appropriate for background conditions above 20 km in the tropics. However, it may be unrepresentative of lidar ratios closer to the tropopause and at mid-to-high latitudes. Future versions of the CALIPSO level 3 stratospheric aerosol profile product may refine the lidar ratios based on these and forthcoming analyses.

Acknowledgements:

J. K. would like to thank Jean-Paul Vernier, M. C. Pitts and Larry Thomason for useful discussions during the development of the CALIPSO stratospheric product. SAGE III aerosol data were obtained from the Langley Atmospheric Science Data Center.

References:

Ansmann, A., Baars, H., Chudnovsky, A., Mattis, I., Veselovskii, I., Haarig, M., Seifert, P., Engelmann, R. and Wandinger, U., Extreme levels of Canadian wildfire smoke in the stratosphere over central Europe on 21-22 August 2017, Atmos. Chem. Phys., 18, 11831-11845, https://doi.org/10.5194/acp-18-11831-2018, 2018.

Beyerle, G., Neuber, R., Schrems, O., Wittrock, F., and Knudsen, B.: Multiwavelength lidar measurements of stratospheric aerosols above Spitsbergen during winter 1992/93, Geophys. Res. Lett., 21, 57-60, https://doi.org/10.1029/93GL02846, 1994.

Brock, C. A., Jonsson, H. H., Wilson, J. C., Dye, J. E., Baumgardner, D., Borrmann, S., Pitts, M. C., Osborn, M. T., Decoursey, R. J. and Woods, D. C.: Relations between optical extinction, backscatter and aerosol surface and volume in the stratosphere following the eruption of Mt. Pinatubo, Geophys. Res. Lett., https://doi.org/10.1029/93GL01691, 1993.

Bourassa, A., Rieger, L. A., Lloyd, N. D. and Degenstein, D. A.: Odin-OSIRIS stratospheric aerosol data product and SAGE III intercomparison, Atmos. Chem. Phys., 12, 605-614, https://doi.org/10.5194/acp-12-605-2012, 2012.

Chazette, P., David, C., Lefrere, J., Godin, S., Pelon, J and Megie, G.: Comparative lidar study of the optical, geometrical and dynamical properties of stratospheric post-volcanic aerosols, following the eruptions of El Chichon and Mount Pinatubo, J. Geophys. Res., 100, D11, 23195-23207, https://doi.org/10.1029/95JD02268, 1995.

Cisewski, M., Zawodny, J., Gasbarre, J., Eckman, R., Topiwala, N., Rodriguez-Alverez, O., Cheek, D. and Hall, S., The Stratospheric Aerosol and Gas Experiment (SAGE III) on the International Space Station (ISS) mission, Proc. of SPIE, 9241, 924107, 2014.

Chen, Z., Bhartia, P. K., Loughman, R., Coloarco, P. and Deland, M., Improvement of stratospheric aerosol extinction retrieval from OMPS/LP using a new aerosol model, Atmos. Meas. Tech., 11, 6495-6509, https://doi.org/10.5194/amt-11-6495-2018, 2018.

Chu, W. P., McCormick, M. P., Lenoble, J., Brogniez, C., and Pruvost, P.: SAGE II inversion algorithm, J. Geophys. Res., 94(D6), 8339–8351, https://doi.org/10.1029/89JD00113, 1989.

Damadeo, R. P., Zawodny, J. M., Thomason, L. W. and Iyer, N., SAGE version 7.0 algorithm: Application to SAGE II, Atmos. Meas. Tech., 6, 3539–3561, https://doi.org/10.5194/amt-6-3539-2013, 2013.

de Laat, A. T. J., Stein Zweers, D. C., Boers, R.. and Tuinder, O. N. E.: A solar escalator: Observational evidence of the self-lifting of smoke and aerosols by absorption of solar radiation in the February 2009 Australian Black Saturday plume, J. Geophys. Res., 117, D04204, https://doi.org/10.1029/2011JD017016, 2012.

Deshler, T.: A review of global stratospheric aerosol: Measurements, importance, life cycle, And local stratospheric aerosol, Atmos. Res., 90, 223-232, https://doi.org/10.1016 /j.atmosres.2008.03.016, 2008.

de Vries, M. J. M. Penning, Dorner, S., Pukite, J., Hormann, C., Formm, M. D. and Wagner, T., Characterisation of a stratospheric sulfate plume from the Nabro volcano using a combination of passive satellite measurements in nadir and limb geometry, Atmos. Chem. Phys., 14, 8149-8163, https://doi.org/10.5194/acp-14-8149-2014, 2014.

Friberg, J., Martinsson, B. G., Andersson, S. M. and Sandvik, O. S., Volcanic impact on the climate—the stratospheric aerosol in the period 2006-2015, Atmos. Chem. Phys., 18, 11149–11169, https://doi.org/10.5194/acp-18-11149-2018, 2018.

Fromm, M., Lindsey, D. T., Servranckx, R., Yue, G., Trickle, T., Sica, R., Doucet, P., and Godin-Beekmann, S., The untold story of pyrocumulonimbus, Bull. American Met. Soc., 1193-1209, https://doi.org/10.1175/2010BAMS3004.1 , 2010.

Gelaro, R., McCarty, W., Suarez, M. J., Todling, R., Molod, A., Takacs, L., Randles, C. A., Darmenov, A., Bosilovich, M. G., Reichle, R., Wargan, K., Coy, L., Cullather, R., Draper, C., Akella, S., Buchard, V., Conaty, A., Da Silva, A. M., Gu, W., Kim, G.-K., Koster, R., Lucchesi, R., Markova, D., Nielsen, J. E., Partyka, G., Pawson, S., Putman, W., Rienecker, M., Schubert, S. C., Sienkiewicz, M., and Zhao, B.: The Modern-Era Retrospective Analysis for Research and Applications, Version 2 (MERRA-2), J. Climate, 30, 5419–5454, https://doi.org/10.1175/JCLI-D-16-0758.1, 2017.

Glatthor, N., Höpfner, M., Semeniuk, K., Lupu, A., Palmer, P. I., McConnell, J. C., Kaminski, J. W., von Clarmann, T., Stiller, G. P., Funke, B., Kellmann, S., Linden, A., and Wiegele, A.: The Australian bushfires of February 2009: MIPAS observations and GEM-AQ model results, Atmos. Chem. Phys., 13, 1637-1658, https://doi.org/10.5194/acp-13-1637-2013, 2013.

Haarig, M., Ansmann, A., Baars, H., Jimenez, C., Veselovskii, I., Engelmann, R., and Althausen, D.: Depolarization and lidar ratios at 355, 532, and 1064 nm and microphysical properties of aged tropospheric and stratospheric Canadian wildfire smoke, Atmos. Chem. Phys., 18, 11847-11861, https://doi.org/10.5194/acp-18-11847-2018, 2018.

Hofmann, D., Barnes, J., O'Neill, M., Trudeau, M., and Neely, R., Increase in background stratospheric aerosol observed with lidar at Mauna Loa observatory and Boulder, Colorado, Geophys. Res. Lett., **36**, L15808, https://doi.org/10.1029/2009GL039008, 2009.

Jaeger, H and Deshler, T., Lidar backscatter to extinction, mass and area conversions for stratospheric aerosols based on midlatitude balloonborne size distribution measurements, Geophys. Res. Lett., 29, 1929, https://doi.org/10.1029/2002GL015609, 2002.

Junge, C. E., and Manson, J. E., Stratospheric aerosol studies, J. Geophys. Res., 66, 2163–2182, https://doi.org/10.1029/JZ066i007p02163, 1961.

Kar, J. Bremer, H., Drummond, J. R., Rochon, Y. J., Jones, D. B. A., Nichitiu, F., Zou, J., Liu, J., Gille, J. C., Edwards, D. P., Deeter, M. N., Francis, G., Ziskin, D. and Warner, J., Evidence of vertical transport of carbon monoxide from Measurements of Pollution in the Troposphere, Geophys. Res. Lett., 31, L23105, https://doi.org/10.1029/2004GL021128, 2004.

Kar, J., Vaughan, M. A., Lee, K.-P., Tackett, J. L., Avery, M. A., Garnier, A., Getzewich, B. J., Hunt, W. H., Josset, D., Liu, Z., Lucker, P. L., Magill, B., Omar, A. H., Pelon, J., Rogers, R. R., Toth, T. D., Trepte, C. R., Vernier, J.-P., Winker, D. M., and Young, S. A.: CALIPSO lidar calibration at 532 nm: version 4 nighttime algorithm, Atmos. Meas. Tech., 11, 1459-1479, https://doi.org/10.5194/amt-11-1459-2018, 2018.

Kar, J., Vaughan, M. A., Tackett, J. Omar, A., Trepte, C. R. and Lucker, P. L., Constrained lidar ratios for volcanic ash and sulfate layers in the stratosphere from CALIOP version 4.10 data, paper presented at the American Geophysical Union Fall Meeting, Washington, DC., Dec.10-14, 2018.

Khaykin, S. M., Godin-Beekmann, S., Keckhut, P., Hauchecorne, A., Jumelet, J., Vernier, J.-P., Bourassa, A., Degenstein, D. A., Rieger, L. A., Bingen, C.,Vanhellemont, F., Robert, C., DeLand, M. and Bhartia, P. K., Variability and evolution of the midlatitude stratospheric aerosol budget from 22 years of ground-based lidar and satellite observations, Atmos. Chem. Phys., 17, 1829–1845, https://doi.org/10.5194/acp-17-1829-2017, 2017.

Khaykin, S. M., Godin-Beekmann, S., Hauchecorne, A., Pelon, J., Ravetta, F. and Keckhut, P., Stratospheric smoke with unprecedentedly high backscatter observed by lidars above southern France, Geophys. Res. Lett., https://doi.org/10.1002/2017GL076763, 2018.

Kremser, S., Thomason, L. W., von Hobe, M., Hermann, M., Deshler,T., Timmreck, C., Toohey, M., Stenke, A., Schwarz, J. P., Weigel, R., Fueglistaler, S., Prata, F. J., Vernier, J.-P., Schlager, H., Barnes, J. E., Antuna-Marrero, J.-C., Fairlie, D., Palm, M., Mahieu, E., Notholt, J., Rex, M., Bingen, C., Vanhellemont, F., Bourassa, A., Plane, J. M. C., Kolcke, D., Carn, S. A., Clarisse, L., Trickl, T., Neely, R., James, A. D., Rieger, L., Wilson,J. C., and Meland, B.: Stratospheric aerosol-Observations, processes and impact on climate, Rev. Geophys., 54, 278–335, https://doi.org/10.1002/2015RG000511, 2016.

Liu, Z., Liu, D., Huang, J., Vaughan, M., Uno, I., Sugimoto, N., Kittaka, C., Trepte, C., Wang, Z, Hostetler, C. and Winker, D., Airborne dust distribution over the Tibetan Plateau and surrounding areas derived from the first year of CALIPSO lidar observations, Atmos. Chem. Phys., 5045-5060, https://doi.org/10.5194/acp-8-5045-2008, 2008.

Liu, Z. Vaughan, M., Winker, D., Kittaka, C., Getzewich, B., Kuehn, R., Omar, A., Powell, K., Trepte, C., and Hostetler, C.: The CALIPSO lidar cloud and aerosol discrimination: Version 2 Algorithm and initial assessment of performance, J. Atmos. Ocean. Tech., 26, 1198–1212, https://doi.org/10.1175/2009JTECHA1229.1, 2009.

Liu, Z., Kar, J., Zeng, S., Tackett, J., Vaughan, M., Avery, M., Pelon, J., Getzewich, B., Lee, K.-P., Magill, B., Omar, A., Lucker, P., Trepte, C., and Winker, D.: Discriminating between clouds and aerosols in the CALIOP version 4.1 data products, Atmos. Meas. Tech., 12, 703-734, https://doi.org/10.5194/amt-12-703-2019, 2019.

Lopes, F. J. S., Silva, J. J., Antuña Marrero, J. C., Taha, G. and Landulfo, E.: Synergetic Aerosol Layer Observation After the 2015 Calbuco Volcanic Eruption Event, Remote Sens., **11**, 195, https://doi.org/10.3390/rs11020195, 2019.

Mauldin III, L. E., Zaun, N. H., McCormick, M. P., Guy, J. H. and Vaughan, W. R.: Stratospheric aerosol and Gas Experiment II instruments: A functional description, Opt. Eng., 24, 307-312, https://doi.org/10.1117/12.7973473, 1985.

McCormick, M. P., Swissler, T. J. , Fuller, , Hunt, W. H. and Osborn, M. T.: Airborne and Ground-Based lidar measurements of the El Chichón stratospheric aerosol from 90°N to 56°S, Geofisica Internacional, 23, 187-221, 1984.

McCormick, M. P., Thomason, L. W. and Trepte, C. R.: Atmospheric effects of the Mt Pinatubo eruption, Nature, 373, 399–404, https://doi.org/10.1038/373399a0, 1995.

McElroy, C. T., Nowlan, C. R., Drummond, J. R., Bernath, P. F., Barton, D. V., Dufour, D. G., Midwinter, C., Hall, R. B., Ogyu, A., Ullberg, A., Wardle, D. I., Kar, J., Zou, J., Nichitiu, F., Boone, C. D., Walker, K. A., and Rowlands, N.: The ACE-MAESTRO instrument on SCISAT: Description, performance, and preliminary results, Appl. Optics, 46(20), 4341–4356, 2007.

McGill, M. J., Vaughan, M. A., Trepte, C. R., Hart, W. D., Hlavka, D. L., Winker, D. M., and Kuehn, R.: Airborne validation of spatial properties measured by the CALIPSO lidar, J. Geophys. Res., 112, D20201, https://doi.org/10.1029/2007JD008768, 2007.

Noel, V., Chepfer, H., Hoareau, C., Reverdy, M., and Cesana, G.: Effects of solar activity on noise in CALIOP profiles above the South Atlantic Anomaly, Atmos. Meas. Tech., 7, 1597-1603, https://doi.org/10.5194/amt-7-1597-2014, 2014.

Northam, G. B., Rosen, J. M., Melfi, S. H., Pepin, T. J., McCormick, M. P., Hofmann D. J. and Fuller, W. H.: Dustsonde and Lidar Measurements of Stratospheric Aerosols: a Comparison, Applied Optics, 13, 2416-2421, https://doi.org/10.1364/AO.13.002416, 1974.

Peterson, D. A., Campbell, J. R., Hyer, E. J., Fromm, M. D., Kablick III, G. P., Cossuth, J. H., and DeLand, M. T.: Wildfire-driven thunderstorms cause a volcano-like stratospheric injection of smoke, npj Climate and Atmospheric Science, 1, https://doi.org/10.1038/s41612-018-0039-3, 2018.

Pitts, M. C., Thomason, L. W., Poole, L. R., and Winker, D. M.: Characterization of Polar Stratospheric Clouds with spaceborne lidar: CALIPSO and the 2006 Antarctic season, Atmos. Chem. Phys., 7, 5207-5228, https://doi.org/10.5194/acp-7-5207-2007, 2007.

Pitts, M. C., Poole, L. R., and Thomason, L. W.: CALIPSO polar stratospheric cloud observations: second-generation detection algorithm and composition discrimination, Atmos. Chem. Phys., 9, 7577-7589, https://doi.org/10.5194/acp-9-7577-2009, 2009.

Powell, K. A., Hostetler, C. A., Liu, Z., Vaughan, M. A., Kuehn, R. A., Hunt, W. H., Lee, K.-P. Trepte, C. R., Rogers, R. R., Young, S. A., and Winker, D. M.: CALIPSO Lidar calibration algorithms. Part I: Nighttime 532 nm parallel channel and 532 nm perpendicular channel,

J. Atmos. Ocean. Tech., 26, 2015–2033, https://doi.org/10.1175/2009JTECHA1242.1, 2009.

Prata, A. T., Young, S. A., Siems, S. T and Manton, M. J., Lidar ratios of stratospheric volcanic ash and sulfate aerosols retrieved from CALIOP measurements, Atmos. Chem. Phys., 17, 8599–8618, https://doi.org/10.5194/acp-17-8599-2017, 2017.

Ridley, D. A., Solomon, S., Barnes, J. E., Burlakov, V. D., Deshler, T., Dolgii, S. I., Herber, A. B., Nagai, T., Neely, R. R., Nevzorov, A. V., Ritter, C., Sakai, T., Santer, B. D., Sato, M., Schmidt, A., Uchino, O., and Vernier, J. P.: Total volcanic stratospheric aerosol optical depths and implications for global climate change, Geophys. Res. Lett., 41, 7763–7769, https://doi.org/10.1002/2014GL061541, 2014.

Robock, A., Volcanic eruptions and climate, Rev. Geophysics, 38(2), 191-219, https://doi.org/10.1029/1998RG000054, 2000.

Sakai, T., Uchino, O., Nagai, N., Liley, B., Morino, I., and Fujimoto, T.: Long-term variation of stratospheric aerosols observed with lidars over Tsukuba, Japan, from 1982 and Lauder, New Zealand, from 1992 to 2015, J. Geophys. Res. Atmos., 121, 10283–10293, https://doi.org/10.1002/2016JD025132, 2016.

Solomon, S., Daniel, J. S., Neely III, R. R., Vernier, J. P., Dutton, E. G. and Thomason, L. W., : The persistently variable “background” stratospheric aerosol layer and global climate change, Sci. Express, https://doi.org/10.1126/science.1206027, 2011.

Thomason, L. W. and Peter, T., Assessment of stratospheric aerosol properties (ASAP), SPARC report no 4, WCRP-124,WMO/TD-No. 1295, 2006.

Thomason, L. W., Pitts, M. C., and Winker, D. M.: CALIPSO observations of stratospheric aerosols: a preliminary assessment, Atmos. Chem. Phys., 7, 5283-5290, https://doi.org/10.5194/acp-7-5283-2007, 2007.

Thomason, L. W., Burton, S. P., Luo, B.-P. and Peter, T., SAGE II measurements of stratospheric aerosol properties at non-volcanic levels, Atmos. Chem. Phys., 8, 983-995, https://doi.org/10.5194/acp-8-983-2008, 2008.

Thomason, L. W., Moore, J. R., Pitts, M. C., Zawodny, J. M. and Chiou, E. W., An evaltuation of the SAGE III version 4 aerosol extinction coefficient and water vapor data products, Atmos. Chem. Phys., 10, 2159-2173, https://doi.org/10.5194/acp-10-2159-2010, 2010.

Thomason, L. W., Ernest, N., Millan, L., Rieger, L., Bourassa, A., Vernier, J.-P., Manney, G., Luo, B., Arfeuille, F. and Peter, T., A global space-based stratospheric aerosol climatology: 1979-2016, Earth Sys. Sci. Data, 10, 469-492, https://doi.org/10.5194/essd-10-469-2018, 2018.

Trickl, T., Giehl, H., Jäger, H., and Vogelmann, H.: 35 yr of stratospheric aerosol measurements at Garmisch-Partenkirchen: from Fuego to Eyjafjallajökull, and beyond, Atmos. Chem. Phys., 13, 5205–5225, https://doi.org/10.5194/acp-13-5205-2013, 2013.

Turco, R. P., Whitten, R. C., Toon, O. B., Pollack, J. B., and Hamill, P.: OCS, stratospheric aerosols and climate, Nature, 283, 283–285, https://doi.org/10.1038/283283a0, 1980.

Winker, D. M., J. Pelon, J. A. Coakley, Jr., S. A. Ackerman, R. J. Charlson, P. R. Colarco, P. Flamant, Q. Fu, R. Hoff, C. Kittaka, T. L. Kubar, H. LeTreut, M. P. McCormick, G. Megie, L. Poole, K. Powell, C. Trepte, M. A. Vaughan, B. A. Wielicki: The CALIPSO Mission: A Global 3D View Of Aerosols And Clouds, Bull. Am. Meteorol. Soc., 91, 1211–1229, https://doi.org/10.1175/2010BAMS3009.1, 2010.

Winker, D. M., Liu, Z., Omar, A., Tackett, J. and Fairlie, D., CALIOP observations of the transport of ash from the Eyjafjallajökull volcano in April 2010, J. Geophys. Res., 117, D00U15, https://doi.org/10.1029/2011JD016499, 2012.

Winker, D. M., J. L. Tackett, B. J. Getzewich, Z. Liu, M. A. Vaughan, and R. R. Rogers, The global 3-D distribution of tropospheric aerosols as characterized by CALIOP, Atmos. Chem. Phys., 13, 3345–3361, https://doi.org/10.5194/acp-133345-2013, 2013.

Vaughan, M. A., Powell, K. A., Kuehn, R. E., Young, S. A., Winker, D. M., Hostetler, C. A., Hunt, W. H., Liu, Z., McGill, M. J., and Getzewitch, B. J.: Fully automated detection of cloud and aerosol layers in the CALIPSO lidar measurements, J. Atmos. Ocean. Tech., 26, 2034–2050, https://doi.org/10.1175/2009JTECHA1228.1, 2009.

Vaughan, M. A., Pitts, M., Trepte, C., Winker, D., Detweiler, P., Garnier, A., Getzewich, B., Hunt, W., Lambeth, J., Lee, K.-P., Lucker, P., Murray, T., Rodier, S., Tremas, T., Bazureau, A., and Pelon, J., Cloud-Aerosol LIDAR Infrared Pathfinder Satellite Observations (CALIPSO) data management system data products catalog, Release 4.10, NASA Langley Research Center Document PC-SCI-503, Hampton, Va., USA, 2016.

Vernier, J. P., Pommereau, J. P., Garnier, A., Pelon, J., Larsen, N., Nielsen, J., Christiansen, T., Cairo, F., Thomason, L. W., Leblanc, T., and McDermid, I. S.: Tropical stratospheric aerosol layer from CALIPSO lidar observations, J. Geophys. Res., 114, D00H10, https://doi.org/10.1029/2009JD011946, 2009.

Vernier, J. P., Thomason, L. W., Pommereau, J.-P., Bourassa, A., Pelon, J., Garnier, A., Hauchecorne, A., Blanot, L., Trepte, C., Degenstein, D. and Vargas, F., Major influence of tropical volcanic eruptions on the stratospheric aerosol layer during the last decade, Geophys. Res. Lett., 38, L12807, https://doi.org/10.1029/2011GL047563, 2011.

Vernier, J.-P., Thomason, L. W. and Kar, J., CALIPSO detection of an Asian tropopause aerosol layer, Geophysical Research Letters, 38, L07804, https://doi.org/10.1029/2010GL046614, 2011.

Vernier , J. P., Fairlie, T. D., Murray, J. J., Tupper, A., Trepte, C., Winker, D., Pelon, J., Garnier, A., Jumelet, J., Pavolonis, M., Omar, A. H. and Powell, K.A., An advanced system to monitor the 3D structure of diffuse volcanic ash clouds, *J. Appl. Meteor. Climatol.*, **52**, 2125-2138, https://doi.org/10.1175/JAMC-D-12-0279.1, 2013.

Vernier, J.-P., Fairlie, T. D., Deshler, T., Natarajan, M., Knepp, T., Foster, K., Weinhold, F. G., Bedka, K. M., Thomason, L. and Trepte, C., In situ and space based observations of the Kelud volcanic plume: The persistence of ash in the lower stratosphere, J. Geophys. Res., 121, 11104-11118, https://doi.org/doi:10.1002/2016JD025344, 2016.

Young, S. A. and Vaughan, M. A.: The retrieval of profiles of particulate extinction from Cloud Aerosol Lidar Infrared Pathfinder Satellite Observations (CALIPSO) data: Algorithm description, J. Atmos. Ocean. Tech., 26, 1105–1119, https://doi.org/10.1175/2008JTECHA1221.1, 2009.

Young, S. A., Vaughan, M. A., Kuehn, R. E., and Winker, D. M.: The retrieval of profiles of particulate extinction from Cloud–Aerosol Lidar Infrared Pathfinder Satellite Observations (CALIPSO) data: Uncertainty and error sensitivity analyses. J. Atmos. Ocean. Tech., 30, 395–428, https://doi.org/10.1175/JTECH-D-12-00046.1, 2013.

Young, S. A., Vaughan, M. A., Kuehn, R. E., and Winker, D. M.: Corrigendum, J. Atmos. Ocean. Tech., 33, 1795–1798, https://doi.org/10.1175/JTECH-D-16-0081.1, 2016.

Young, S. A., Vaughan, M. A., Garnier, A., Tackett, J. L., Lambeth, J. D., and Powell, K. A.: Extinction and optical depth retrievals for CALIPSO's Version 4 data release, Atmos. Meas. Tech., 11, 5701-5727, https://doi.org/10.5194/amt-11-5701-2018, 2018.